Reciprocal Control of Motility and Biofilm Formation by the PdhS2 Two-Component Sensor Kinase of *Agrobacterium tumefaciens*

Jason E. Heindl[1,2], Daniel Crosby[2], Sukhdev Brar[2], Daniel Merenich[2], Aaron M. Buechlein[3], Eric L. Bruger[4], Christopher M. Waters[4] and Clay Fuqua[1*]

[1]Department of Biology
Indiana University
Bloomington, IN 47405, USA

[2]Department of Biological Sciences
University of the Sciences
Philadelphia, PA 19104, USA

[3]Center for Genomics and Bioinformatics
Indiana University
Bloomington, IN 47405

[4]Department of Microbiology and Molecular Genetics
Michigan State University
East Lansing, MI 48824, USA

Running title: *Agrobacterium* PdhS2 regulates motility and biofilms

Keywords: Development, sensor kinase, phosphorelay, *Agrobacterium tumefaciens*, biofilm, motility

*Address for correspondence: Clay Fuqua, Dept. Biol., 1001 E. 3rd St., Jordan Hall 142, Indiana Univ., Bloomington, IN 47405-1847. Tel: 812-856-6005, FAX: 812-855-6705, E-mail: cfuqua@indiana.edu

Current addresses: J.E.H., Dept. Biol. Sci., Univ. Sci, Philadelphia, PA

ABSTRACT

A core phosphorelay pathway that directs developmental transitions and cellular asymmetries in *Agrobacterium tumefaciens* putatively includes two overlapping, integrated phosphorelays. One of these phosphorelays putatively includes at least four histidine sensor kinase homologues, DivJ, PleC, PdhS1, and PdhS2, and at least two response regulators, DivK and PleD. Previously we demonstrated that PdhS2 reciprocally regulates biofilm formation and swimming motility. In the current study we further dissect the role and regulatory impact of PdhS2 in *A. tumefaciens* revealing that PdhS2-dependent effects on attachment and motility require the response regulator, DivK, but do not require PdhS2 autokinase or phosphotransfer activities. We also demonstrate that PdhS2 regulation of biofilm formation is dependent upon multiple diguanylate cyclases, including PleD, DgcA, and DgcB, implying that PdhS2 regulation of this process intersects with pathways regulating levels of the second messenger cyclic diguanylate monophosphate (cdGMP). Finally, we show that upon cell division a GFP fusion to PdhS2 dynamically localizes to the new pole of the bacterium suggesting that PdhS2 controls processes in the daughter cell compartment of predivisional cells. These observations suggest that PdhS2 negatively regulates DivK, and possibly PleD, activity to control developmental processes in the daughter cell compartment of predivisional cells, as well as in newly released motile daughter cells.

IMPORTANCE

Bacterial developmental processes, including morphological transformations as well as behavioral transitions, are tightly regulated. In many Alphaproteobacteria cell division and development are coordinated by a suite of conserved histidine kinases and their partnered regulatory proteins. Here we describe how the histidine kinase PdhS2 genetically interacts with a single-domain response regulator, DivK, and the intracellular signal cyclic diguanylate monophosphate. PdhS2 dynamically localizes to the new pole of recently divided cells and negatively regulates processes that ultimately lead to attachment and subsequent biofilm formation in *Agrobacterium tumefaciens*. These findings expand our understanding of the links between cell division and developmental control in *A. tumefaciens* and related Alphaproteobacteria.

INTRODUCTION

Bacteria are sometimes considered to be elementary life forms, with simple body plans, streamlined reproductive cycles, and monolithic behavior when compared with higher eukaryotes. To the contrary, many bacteria can exhibit a remarkable diversity of developmental complexity, both temporal and morphological (1, 2). Even bacterial species whose cells appear morphologically uniform, such as rod-shaped *Escherichia coli* or coccoid *Staphylococcus aureus,* possess distinct cellular architectures as well as intricately timed cell division programs, and a large number of bacteria can form multicellular biofilms (3, 4). Developmental processes in bacteria, as in higher eukaryotes, are driven by factors that may be considered both cell-intrinsic and cell-extrinsic. Intrinsic factors include genomic and proteomic content, while extrinsic factors comprise environmental conditions, such as pH and temperature, which cells sense and to which they respond (5).

Members of the Alphaproteobacteria class include host-associated pathogens (*e.g. Brucella* sp., *Bartonella* sp.), host-associated commensals (*e.g. Sinorhizobium* sp., *Bradyrhizobium* sp.), and free-living aquatic bacteria (*e.g. Caulobacter* sp., *Rhodobacter* sp.). Recent work has revealed that several Alphaproteobacteria divide asymmetrically, in which cells elongate, duplicate and segregate their genomic content between two non-equivalent compartments of predivisional cells, and finally generate two cells by cytokinesis (6, 7). Notably, cellular components are unevenly distributed between the two daughter cells during cell division, including surface structures (*e.g.* flagella and holdfasts), cell wall components (*e.g.* peptidoglycan), and even cytoplasmic complexes (*e.g.* heat shock proteins). For example, there may be a clear segregation of existing

organelles to one daughter cell while the second cell generates these structures *de novo* (6, 8-10). Although the specific details may vary among species, the end result is the production of a young daughter cell and a comparatively older mother cell. Not only does this uneven division partition senescence among the products of cell division, but it also allows for the generation of functionally distinct cell types. For example, in *Caulobacter crescentus* the non-motile stalked cell type can attach to surfaces using its polar adhesin called the holdfast (11). This stalked cell then serves as the mother cell during multiple rounds of cell division, generating and releasing motile swarmer cells upon each cytokinetic event (12). Motile swarmer cells are prohibited from entering the cell division cycle until differentiation into the non-motile stalked form (13, 14).

Underlying asymmetric cell division is subcellular differentiation that includes localization of specific regulatory proteins to programmed locations within each cell (15). Prominent among these are components of two overlapping phosphorelays, the first which functions through the response regulators DivK and PleD (the DivK-PleD relay) and the second which functions primarily through the response regulator CtrA (the CtrA relay). The pathways are connected through DivK, which controls initiation of the CtrA relay by regulating the CckA sensor kinase (16, 17). Collectively we refer to these two relays as the DivK-CtrA pathway. In *C. crescentus* the sensor histidine kinases PleC and DivJ control the phosphorylation state of DivK and PleD, and localize to opposing poles of the predivisional cell (18-21). Through antagonistic kinase and phosphatase activities on the same target proteins, DivK and PleD, PleC and DivJ inversely manifest their activity on the most downstream component of the DivK-CtrA pathway, the response regulator CtrA (22-25). DivJ is retained at the stalked cell pole and serves as

a DivK/PleD kinase, resulting in increased DivK~P concentration and decreased CtrA~P concentration in this region of the cell (Fig. 1A). Conversely, PleC localizes to the pole distal to the stalk, where the single polar flagellum is assembled, and where PleC dephosphorylates DivK, leading downstream to increased CtrA~P levels and activity. Phospho-CtrA binds to the replication origin thereby preventing DNA replication and also acts as a transcriptional regulator for many genes, including activating those for assembly of the flagella (26-28). The CtrA relay is also influenced by the DivK-PleD relay through levels of the second messenger cyclic diguanylate monophosphate (cdGMP). DivJ-dependent phosphorylation of PleD at the stalk pole of the predivisional cell stimulates its diguanylate cyclase activity, resulting in higher levels of cdGMP at this end of the cell. The CckA kinase that initiates the CtrA relay is biased away from its kinase and towards its phosphatase activity by direct allosteric control through high levels of cdGMP, thereby reinforcing a CtrA~P gradient, relatively low at the stalk pole and increasing towards the distal pole (29-34) (Fig. 1A).

Agrobacterium tumefaciens is a plant pathogen of the Alphaproteobacteria group that is not stalked, but like *C. crescentus*, divides asymmetrically generating a motile daughter cell from a mother cell (6). As a facultative pathogen, the *A. tumefaciens* lifestyle substantially differs from that of the freshwater oligotroph *C. crescentus*. Nonetheless core components of the DivK-CtrA pathway are well conserved in *A. tumefaciens*, including the three non-essential PleC/DivJ homologue sensor kinase (PdhS) homologues PleC (Atu0982), PdhS1 (Atu0614), and PdhS2 (Atu1888). The *divJ* gene (Atu0921) is essential in *A. tumefaciens* (35, 36) (Fig. 1B). We have previously shown that the three non-essential PdhS homologues have distinct roles in the normal

136 cellular development of *A. tumefaciens* (Kim, 2013). PleC and PdhS1, as well as the *A.*
137 *tumefaciens* DivK homologue, all manifested marked effects on both cell division and
138 complex behaviors including motility and biofilm formation. In genetic backgrounds with
139 reduced or absent levels of these proteins cells are elongated and branched, and these
140 strains also exhibit both reduced motility and reduced biofilm formation. To date the
141 essentiality of *divJ* has precluded exhaustive phenotypic analysis (35) although
142 preliminary depletion studies suggest it similarly impacts these same phenotypes
143 (Heindl et al. in prep). The fourth PdhS family member, PdhS2, does not appear to
144 participate in regulation of cell division as all cells are morphologically wild-type in
145 appearance (35). Loss of PdhS2, however, results in dramatically increased attachment
146 and biofilm formation and simultaneous loss of motility. Reciprocal regulation of these
147 phenotypes is often a hallmark of regulation by cdGMP (37). In this work we further
148 explore the mechanism by which PdhS2 regulates adhesion and motility. Our results
149 link DivK downstream of PdhS2. We also show a clear intersection of PdhS2 activity
150 and the activity of several diguanylate cyclases, suggesting that PdhS2 and cdGMP
151 coordinately regulate biofilm formation and motility in *A. tumefaciens*. Finally, we find
152 that PdhS2 dynamically localizes to the newly generated poles of both the new daughter
153 cell and the mother cell following cytokinesis. This pattern suggests that PdhS2 activity
154 is specifically required for proper development of motile daughter cells.
155

RESULTS

DivK is epistatic to PdhS2. Members of the PdhS family of sensor kinases were originally identified based on homology with their namesakes DivJ and PleC of *C. crescentus* (38, 39) (Fig. 1B). Based on this homology all PdhS family members are predicted to interact with the single domain response regulator DivK (39) and also interact with the diguanylate cyclase response regulator PleD. Prior work from our laboratory has shown that both swimming motility and adherent biomass are diminished in the Δ*divK* mutant, implying that DivK activity is required for proper regulation of these phenotypes in *A. tumefaciens* (35). In contrast, the PdhS–type kinase PdhS2 inversely regulates these phenotypes; a Δ*pdhS2* mutant is non-motile but hyperadherent (35). To determine whether PdhS2 genetically interacts with DivK we constructed a Δ*divK*Δ*pdhS2* mutant and compared swimming motility and biofilm formation in this strain to wild-type and parental single deletion strains (Fig. 2A). As seen before, loss of either *divK* or *pdhS2* reduced swimming motility as measured by swim ring diameter on motility agar. Biofilm formation on PVC coverslips in the Δ*divK* mutant was reduced relative to the wild-type C58 strain while for the Δ*pdhS2* mutant it was dramatically increased. The Δ*divK*Δ*pdhS2* mutant phenocopied the Δ*divK* mutant in both assays, with no significant difference in the efficiency of either swimming motility or biofilm formation between the two strains.

Swim ring diameters of the Δ*divK* and Δ*divK*Δ*pdhS2* mutants were decreased by roughly 20% compared to wildtype while the decrease in Δ*pdhS2* swim ring diameters was roughly 40% compared to wildtype, suggesting that the nature of the defect in swimming motility differs between these two classes of mutants and that loss of *divK*

179 partially restores motility in the absence of *pdhS2*. Indeed, it was earlier noted that while
180 both the Δ*divK* and the Δ*pdhS2* single deletion mutants produce polar flagella few
181 Δ*pdhS2* mutant bacteria were observed to be motile under wet-mount microscopy
182 implying that the swimming defect is due to diminished flagellar activity rather than
183 flagellar assembly (35). The Δ*divK* mutant, however, was readily observed to be motile
184 under wet-mount microscopy. Similarly, the Δ*divK*Δ*pdhS2* mutant generates polar
185 flagella and its motility is readily observed under wet-mount microscopy (data not
186 shown). Both the Δ*divK* and Δ*divK*Δ*pdhS2* mutants, and not the Δ*pdhS2* mutant,
187 generate aberrant cell morphologies including elongated and branched cells (35) (Data
188 not shown). These data support the hypothesis that PdhS2 interacts with DivK and that
189 the phenotypes of the Δ*pdhS2* mutant are at least partly due to altered regulation of
190 DivK activity. Moreover, the reciprocal nature of the phenotypes between the Δ*divK* and
191 Δ*pdhS2* mutants implies that PdhS2 negatively regulates DivK.

192 Further support for PdhS2 activity proceeding through DivK was provided by
193 expressing wild-type PdhS2 ectopically from a P_{lac} promoter. Induced expression of
194 *pdhS2* rescues swimming motility and returns biofilm formation closer to wild type levels
195 in the Δ*pdhS2* mutant, albeit incompletely (Fig. 2B). However, as predicted from the
196 Δ*divK*Δ*pdhS2* phenotypes, plasmid-borne provision of PdhS2 in the Δ*divK* mutant had
197 no significant effect on either biofilm formation or swimming motility (Fig. 2C).

198

199 **PdhS2 kinase and phosphatase activities coordinately regulate developmental**
200 **phenotypes.** Members of the PdhS family of sensor histidine kinases contain a
201 conserved HATPase_c catalytic domain at their carboxyl termini and an upstream

conserved HisKA dimerization/phosphoacceptor domain (Fig. 1C). Many sensor kinases exhibit bifunctional catalytic activity, alternately acting as kinase or phosphatase, and in *C. crescentus* PleC is one such example (18, 22, 40). Multiple sequence alignment of the HisKA domain from the *A. tumefaciens* and *C. crescentus* PdhS family kinase homologues highlights the high level of conservation of this domain including the phospho-accepting histidine residue (H271 of PdhS2) and a threonine residue important for phosphatase activity (T275 of PdhS2) (Fig. 1B).

To test the requirement of the conserved phospho-accepting histidine for PdhS2 activity we mutated this residue to alanine (H271A) and evaluated the ability of this mutant *pdhS2* allele to complement Δ*pdhS2* phenotypes (Fig. 2B). Ectopic expression of PdhS2^{H271A} (P_{lac}-*pdhS2* on a low copy plasmid) efficiently complemented the attachment and motility phenotypes of the Δ*pdhS2* mutant. These data indicate that this histidine residue is not required for PdhS2 regulation of swimming motility and biofilm formation, and imply that PdhS2 autokinase and phosphotransfer are not required to regulate these phenotypes. Instead, we hypothesize that PdhS2 acts primarily as a phosphatase towards its cognate response regulators, including DivK.

The conserved HisKA dimerization/phosphoacceptor domain is also primarily responsible for the phosphatase activity of these two-component system kinases (41). Phosphatase activity requires a conserved threonine residue roughly one α-helical turn (4 residues) downstream of the phospho-accepting histidine residue. To test the requirement for PdhS2 phosphatase activity in regulating developmental phenotypes we mutated this conserved threonine residue to alanine (Thr275A) and evaluated the ability of this mutant *pdhS2* allele to complement Δ*pdhS2* phenotypes. In contrast to the

PdhS2^{H271A} mutant protein, equivalent ectopic expression of the PdhS2^{T275A} allele failed to complement the Δ*pdhS2* motility and attachment phenotypes, and in fact exacerbated them (Fig. 2B). Expression of either the kinase-null or the phosphatase-null allele of PdhS2 in the Δ*divK* background had no effect on biofilm formation or swimming motility (Fig. 2C). A PdhS2 double mutant with both the histidine and threonine residues mutated had no effect on biofilm formation or swimming motility (Fig. S1). Together these data are most consistent with the hypothesis that PdhS2 phosphatase activity is primarily responsible for regulating these phenotypes in *A. tumefaciens*. The data are also consistent with PdhS2 negatively regulating DivK, and DivK being downstream of PdhS2 in the DivK-CtrA pathway. In wild-type *A. tumefaciens* induced expression of PdhS2 modestly but significantly increases biofilm formation and decreases swimming motility (Fig. 2B). Induced expression of the PdhS2^{H271A} protein in the wild-type background, however, significantly reduces biofilm formation. These data suggest that PdhS2 kinase activity may also play a role during the normal life cycle of *A. tumefaciens* and that the balance of PdhS2 kinase and phosphatase activities is coordinated to match dynamic cellular conditions.

PdhS2 and DivJ localize to the pole of *A. tumefaciens*. One mechanism for establishing and maintaining developmental asymmetries in bacteria is the differential polar localization of proteins with opposing functionalities (42, 43). Several members of the PdhS family of sensor kinases localize to one or both bacterial poles (18, 22, 44). Using a full length PdhS2-GFP fusion that retains wild type functionality we tracked localization of PdhS2 in *A. tumefaciens* following induction of expression with IPTG (Fig.

3A and Movie S1). In both wild-type and Δ*pdhS2* backgrounds PdhS2-GFP localized primarily to the budding pole of predivisional cells. Time-lapse microscopy of the Δ*pdhS2* mutant expressing PdhS2-GFP revealed apparent dynamic relocalization of PdhS2-GFP to the newly generated pole of the daughter cell coincident with cytokinesis. In the mother cell a new focus of PdhS2-GFP subsequently accumulates at the new budding pole generated following septation and daughter cell release. These time-lapse experiments clearly indicate that PdhS2-GFP localizes to the actively budding pole of the cell, and is lost at that pole as it matures and the cell proceeds to the predivisional state. Following cytokinesis PdhS2-GFP localizes to the newly generated, younger poles of both the daughter cell and the mother cell. This dynamic localization is consistent with PdhS2 activity being restricted to the motile-cell compartment of predivisional cells and to newly generated motile cells.

Since PdhS2 localizes to the budding pole of dividing cells and primarily requires its phosphatase activity there likely exist one or more non-budding pole-localized kinases opposing PdhS2 activity. The most obvious candidate for this activity is DivJ. DivJ localizes to the old pole in *C. crescentus* and acts as a DivK kinase in both *C. crescentus* and *S. meliloti* (39, 45). Time-lapse microscopy of a full length DivJ-GFP fusion in wild-type *A. tumefaciens* reveals localization to the non-budding pole in mother cells that is not redistributed over the course of multiple cell division cycles (Fig. 3B and Movie S2). The interplay between PdhS2 and DivJ is a topic of current study, one made difficult by the essential nature of *divJ*. The remaining PdhS kinases also likely affect DivK or PleD activity. Localization patterns for PdhS1 and PleC have not been determined. However, phenotypic evaluation of *pdhS1*, *pdhS2*, and *pleC* double and

triple mutants reveals complicated and non-redundant regulation of biofilm formation by these PdhS kinases (Fig. S2).

PdhS2 and DivK affect CtrA activity. To determine the effect of PdhS2 and DivK activity on CtrA activity and stability in *A. tumefaciens* we evaluated its steady-state levels and turnover in unsynchronized cells. Steady-state levels of CtrA protein measured in stationary phase cultures were modestly increased in the Δ*pdhS2* background and modestly decreased in the Δ*divK* background, consistent with PdhS2 and DivK inversely regulating CtrA accumulation or stability (Fig. 4A). Because steady-state protein levels reflect the balance between protein synthesis and degradation CtrA protein stability was evaluated following treatment of cultures with chloramphenicol to inhibit translation. In wild-type cultures, translation inhibition leads to a decline in CtrA abundance over the course of 2-3 hours, diminishing to roughly 30% of the steady-state levels. Loss of *pdhS2* had no effect on either final steady-state levels of CtrA following inhibition of translation or the observed rate of turnover when compared with wild-type cultures (Fig. 4B). Taken together these data suggest that PdhS2 and DivK are likely to primarily affect CtrA activity or accumulation rather than CtrA stability.

In *C. crescentus*, CtrA is known to directly regulate at least 55 operons, acting as either an activator or repressor of transcription (22, 28). *A. tumefaciens* CtrA is predicted to act similarly to *C. crescentus* CtrA, binding to DNA in a phosphorylation-dependent manner and regulating DNA replication and transcription. *A. tumefaciens* CtrA is 84% identical to *C. crescentus* CtrA at the amino acid level and purified *C. crescentus* CtrA binds to a site upstream of the *A. tumefaciens ccrM* gene (46).

Furthermore, computational analysis of multiple Alphaproteobacterial genomes uncovered numerous cell cycle regulated genes preceded by a consensus CtrA binding site (47). We therefore evaluated CtrA activity by determining the transcriptional activity of several known and hypothesized CtrA-dependent promoters from both *C. crescentus* and *A. tumefaciens*. The *ccrM*, *ctrA*, and *pilA* promoters from *C. crescentus* were chosen to represent CtrA-activated promoters that we predicted would be similarly regulated in *A. tumefaciens* (13, 14, 48, 49). In the Δ*pdhS2* background, expression levels from both the *ctrA* and *pilA* promoters from *C. crescentus* were significantly reduced while transcription from the *C. crescentus ccrM* promoter was unchanged (Table 1). In the *A. tumefaciens* Δ*divK* background the *C. crescentus ccrM* and *ctrA* promoters exhibited increased activity while the *pilA* promoter was unchanged (Table 1). These data are largely consistent with *A. tumefaciens* CtrA regulating transcription of known CtrA-dependent promoters, and with PdhS2 and DivK inversely regulating CtrA activity in *A. tumefaciens*.

From *A. tumefaciens* the *ccrM* promoter is the only promoter for which experimental data suggest CtrA-dependent regulation, thus this promoter was selected for analysis (46). Curiously, the same computational analysis that identified possible CtrA-dependent promoters among a suite of Alphaproteobacterial genomes failed to find a significant CtrA binding motif upstream of the *A. tumefaciens ccrM* gene (47). In addition to *ccrM*, putative promoters for *ctrA* and *pdhS1* were selected for analysis based on the presence of at least one predicted CtrA binding site as well as hypothesized cell cycle regulation of these loci. Transcriptional activity from the *A. tumefaciens ctrA* and *pdhS1* promoter constructs showed inverse regulation in the

317 Δ*pdhS2* and Δ*divK* backgrounds, with expression decreased from the *ctrA* promoter and
318 increased at the *pdhS1* promoter in the Δ*pdhS2* mutant, and exactly reversed in the
319 Δ*divK* mutant. Although absence of *pdhS2* had little effect on the *A. tumefaciens ccrM*
320 promoter, transcription from this promoter was significantly increased in the Δ*divK*
321 background (Table 1). These data are congruent with the above data for *C. crescentus*
322 CtrA-dependent promoters and further support CtrA regulation of cell cycle-responsive
323 genes in *A. tumefaciens*.
324
325 **PdhS2 activity intersects with cyclic-di-GMP pools.** In *C. crescentus* DivJ and PleC
326 positively regulate, via phosphorylation, a second response regulator, PleD, as well as
327 DivK (22). In *C. crescentus* and *A. tumefaciens* the *divK* and *pleD* coding sequences
328 form one operon and transcriptional regulation of both genes is linked. Since PdhS
329 kinases are predicted to interact with both DivK and PleD we analyzed the effect of loss
330 of PleD activity in the Δ*pdhS2* background. As reported previously, deletion of *pleD*
331 alone has minimal effect on either swimming motility or adherent biomass (35). Loss of
332 *pleD* in the Δ*pdhS2* background had only a minor effect on swimming motility (Fig.
333 S3A). Adherent biomass, however, was reduced by approximately 30%, indicating that
334 PleD contributes to the increased attachment phenotype of the Δ*pdhS2* mutant (Fig.
335 5A).
336 PleD is a GGDEF motif-containing diguanylate cyclase, and thus it is likely that
337 the attachment phenotype of the Δ*pdhS2* mutant requires increased levels of cdGMP.
338 Earlier work from our lab identified three additional diguanylate cyclases that are
339 relevant to attachment and biofilm formation: DgcA, DgcB, and DgcC (50) (Wang

unpublished). As seen in wild-type C58, deletion of *dgcA* or *dgcB* in the Δ*pdhS2* background significantly decreased attachment and biofilm formation, whereas loss of *dgcC* did not (Fig. 5A). These data suggest that increased biofilm formation by the Δ*pdhS2* mutant is dependent on cdGMP pools, generated through PleD, DgcA, and DgcB. Swimming motility was equivalent in either wild-type C58 or Δ*pdhS2* backgrounds in combination with mutations in *pleD*, *dgcA*, *dgcB*, or *dgcC* (Fig. S3A).

Previously we found that mutants lacking either *dgcA*, *dgcB*, or *dgcC* show no difference in average levels of cdGMP (50). Nonetheless, loss of either *dgcA* or *dgcB*, or mutation of the GGDEF catalytic site of either enzyme, significantly reduced biofilm formation (50), implicating these enzymes in controlling the pool of cdGMP, and affecting attachment. We compared cytoplasmic cdGMP levels among wild-type C58, the Δ*pdhS2* mutant, and the Δ*pdhS2* Δ*dgcB* mutant strain and found no change in these levels (Fig. S4). To verify that the diguanylate cyclase (DGC) activity is responsible for the increased biofilm formation in the Δ*pdhS2* background we expressed an allele of *dgcB* with a mutation in its GGDEF catalytic motif (GGAAF; *dgcB**). We have previously shown that this mutation abrogates cdGMP formation by DgcB and that production of this mutant protein does not complement a Δ*dgcB* mutant for either cdGMP formation or attachment phenotypes (50). Plasmid-borne expression of wild-type *dgcB* (P_{lac}-*dgcB*) results in a massive increase in attachment and biofilm formation in either the wild-type C58 or Δ*pdhS2* background (Fig. 5B). Expression of *dgcB** from a P_{lac} promoter, however, did not increase biofilm formation in either background. In the Δ*pdhS2* Δ*dgcB* mutant background expression of wild-type *dgcB* increased biofilm formation to the same degree seen in the wild-type and Δ*pdhS2* mutant. Expression of the mutant *dgcB**

363 allele in the Δ*pdhS2* Δ*dgcB* mutant did appear to modestly increase biofilm formation,
364 although far less than with the wild-type *dgcB* allele. Swimming motility was modestly
365 but significantly reduced when the wild-type *dgcB* allele was provided *in trans* (Fig.
366 S3B). Together these data are consistent both with PdhS2 negatively regulating one or
367 more diguanylate cyclases, and for increased synthesis of cdGMP mediating the
368 attachment and biofilm formation phenotypes of the Δ*pdhS2* mutant and contributing,
369 albeit less so, to the Δ*pdhS2* motility phenotype.
370
371 **Increased attachment in a pdhS2 mutant requires the UPP polysaccharide**. We
372 have previously reported that PleD-stimulated attachment was due to increased levels
373 of the unipolar polysaccharide (UPP) and cellulose (50). In addition to UPP and
374 cellulose, *A. tumefaciens* produces at least three other exopolysaccharides:
375 succinoglycan, cyclic β-1, 2 glucans, β-1, 3 glucan (curdlan), as well as outer membrane
376 associated lipopolysaccharide (LPS) (51). Of these only LPS is essential for *A.*
377 *tumefaciens* growth (36). The Δ*pdhS2* strain was tested for the impact of each of the
378 non-essential exopolysaccharides for biofilm formation. The *upp* mutation completely
379 abolished attachment in both the wild type and the *pdhS2* mutant (Fig. S5). The *chvAB*
380 mutant, known to have pleiotropic effects (52), was diminished in adherence overall, but
381 was still elevated by the *pdhS2* mutation. None of the other exopolysaccharide
382 pathways impacted adherence in either background. These results confirm that biofilm
383 formation in the Δ*pdhS2* strain is dependent primarily on UPP and that the motility
384 phenotype of the Δ*pdhS2* mutant is not dependent on any of the known
385 exopolysaccharides.

Global transcriptional analysis of PdhS2 activity. Prior work on the DivK-CtrA pathway in other Alphaproteobacteria has shown that one mechanism by which these bacteria switch between the developmental programs of mother and daughter cells is by differential gene expression in the two cell types (27, 39, 53). The PdhS kinases may affect gene expression through two mechanisms. First, members of the PdhS kinase family have been demonstrated to affect the activity of the global transcriptional regulator, CtrA, in several Alphaproteobacteria, including *C. crescentus*, *S. meliloti*, and *B. abortus* (32, 39, 44, 54). Transcriptome effects may also result from partitioning during cytokinesis of factors regulating transcription independent of CtrA, a process that is itself indirectly regulated by the PdhS family kinases. To determine the effect of PdhS2 activity on the *A. tumefaciens* transcriptome we used whole genome microarrays. Gene expression was compared between WT and Δ*pdhS2* strains grown to exponential phase in minimal media. Of 5338 unique loci represented on the arrays 39 genes were differentially regulated above our statistical cut-offs (P values, ≤ 0.05; $\log_2$ ratios of ≥ ± 0.50; Table 2). Of these, 24 genes were significantly upregulated, indicating negative regulation by PdhS2. Upregulated genes included *dgcB*, shown above to contribute to biofilm formation in the Δ*pdhS2* mutant, and Atu3318, a LuxR-type transcriptional regulator previously identified as regulated by the VisNR regulatory system involved in motility and biofilm formation (50). Downregulated genes included six succinoglycan biosynthetic genes, consistent with previously published results showing positive regulation of succinoglycan production by PdhS2 (35).

To determine whether any of these 39 genes were putatively regulated by CtrA we scanned a sequence window from 500 bp upstream of the start codon to 100 bp into the coding sequence for plausible CtrA binding sites. CtrA binding sites were defined using the conserved Alphaproteobacterial CtrA recognition sequence 5'-TTAANNNNNNGTTAAC-3' (46, 47). Sequences containing seven or more of the conserved nucleotides in this motif were deemed plausible candidates. Using these parameters 16 differentially transcribed loci have matching upstream sequences and are thus putatively regulated by CtrA, including *dgcB* and Atu3318, as well as all five of the downregulated succinoglycan biosynthetic genes (Table 2).

To verify our microarray results we measured transcription of translational fusions to β-galactosidase from two selected genes, *dgcB* and Atu3318, in wild-type and Δ*pdhS2* backgrounds (Table 1). In both cases beta-galactosidase activity increased in the Δ*pdhS2* mutant, corroborating the microarray results. Overall these results are consistent with PdhS2 impacting the motile cell developmental program through transcriptional control. The data are also consistent with PdhS2 negatively regulating DivK and thereby indirectly affecting CtrA activity during the *A. tumefaciens* cell cycle.

DISCUSSION

PdhS2 is a key regulator of developmental phenotypes. Regulation of the developmental program of many Alphaproteobacteria centers on the global transcriptional regulator CtrA (42, 47, 55, 56). CtrA activity is controlled, indirectly, through a series of phosphotransfer reactions dependent on one or more PdhS-type histidine kinases. Here we show that PdhS2, one of at least four PdhS family kinases from *A. tumefaciens*, regulates developmental phenotypes at least in part through fine-tuning of the activity of CtrA. We demonstrate that null mutations of the single domain response regulator *divK* are epistatic to *pdhS2* in *A. tumefaciens* and that PdhS2 is likely to negatively regulate DivK activity. Null mutation of a second response regulator, *pleD*, is also epistatic to the *pdhS2* mutation. The phosphatase activity of PdhS2 predominates *in vivo*, although it is apparent that its kinase activity is also required for proper regulation of PdhS2 phenotypes. Determination of the timing, specificity, and regulation of both phosphatase and kinase activities await further experimentation. PdhS2 dynamically localizes to the budding pole of *A. tumefaciens* cells following cytokinesis while DivJ, another PdhS-type kinase, localizes to the non-budding pole of each cell. We propose that together the antagonistic activities of DivJ and PdhS2 (and perhaps additional PdhS homologues), coupled with their distinct localization patterns, generate a spatiotemporal gradient of phospho-DivK and phospho-PleD and an opposing gradient of phospho-CtrA, thus differentially regulating the developmental program of *A. tumefaciens* (Fig. 1A). Computational models of asymmetric cell development in *C. crescentus* support this notion, with the important *caveat* that

447 phospho-DivK and phospho-PleD may not be distributed in a gradient but rather locally
448 restricted (23, 25, 57).
449
450 **Plasticity and robustness of the DivK-PleD signaling module and PdhS kinases.**
451 The PdhS kinase homologues are all predicted to interact with two response regulators,
452 DivK and PleD. Through modulating DivK and PleD activity, PdhS family members
453 ultimately affect activity of CtrA. Among the Alphaproteobacteria, regulation of CtrA
454 activity has diversified such that the number of PdhS homologues has increased and/or
455 decreased in different species. Species have been identified that putatively contain as
456 many as 12 distinct members, while other species have lost all PleC/DivJ homologues
457 (39, 47). The *A. tumefaciens* genome encodes four PdhS–type proteins, all of which
458 impact one or more developmental phenotypes. The selective forces leading to
459 expansion or contraction of the number of PdhS family members in different species are
460 unknown. It is evident, however, that simple functional redundancy is not a sufficient
461 explanation as the essentiality and genetic interactions between PdhS family members
462 and their downstream targets (DivK and PleD) varies among different
463 Alphaproteobacteria. In *A. tumefaciens* only *divJ* is essential among the PdhS-type
464 kinases, and neither *divK* nor *pleD* are essential, leading to the hypothesis that at least
465 one unidentified target for DivJ exists, the activity of which is required for viability, or that
466 dysregulation of multiple targets is synthetically lethal (35). All possible single, double,
467 and triple mutant combinations of the remaining PdhS family members in *A.*
468 *tumefaciens* are viable, as is the Δ*divK* Δ*pleD* mutant strain (35) (Fig. S2; and data not
469 shown). The *divK* gene is essential in both *C. crescentus* and *S. meliloti* but essentiality

varies for the PdhS-type kinases (39, 58). Neither *pleC* nor *divJ* are essential in *C. crescentus*, whereas *pleC* is essential in *S. meliloti*. While neither *S. meliloti divJ* nor *cbrA* (another PdhS family member) are independently essential, cells must have at least one copy of either gene for viability (39). The varied essentiality of module components together with the known effects from loss of multiple components highlight both the genetic plasticity and signaling robustness evident in the PdhS-DivK regulatory circuit among Alphaproteobacteria.

PdhS2 influences cdGMP-dependent phenotypes. The effects of the *pdhS2* mutation on biofilm formation and swimming motility by PdhS2 differ from those observed for either the Δ*pleC* or Δ*pdhS1* mutants (35) (and data not shown). In these mutants, biofilm formation is inhibited and cell morphology is elongated and branched, similarly to the Δ*divK* mutant. Reduced swimming motility in these morphologically aberrant cells is most likely due to a combination of their aberrant cell shape and flagellar placement, rather than a defect in assembly or function of the flagella (35). The motility defect in the Δ*pdhS2* strain, however, appears fundamentally distinct. The increased biofilm formation and diminished motility in a *pdhS2* mutant is most similar to the inverse regulation frequently achieved by modulating internal pools of cdGMP. Indeed, our data demonstrate a strong dependence on cdGMP levels for mediating the Δ*pdhS2* phenotypes. Although the overall levels of cdGMP are not significantly affected by the *pdhS2* mutation, it is clear that mutations in the diguanylate cyclases PleD, DgcA and DgcB that disable their ability to synthesize cdGMP diminish the biofilm phenotype of *pdhS2* null mutants. This suggests that increased cdGMP synthesis via these

493 enzymes may impart the effects on motility and biofilm formation. PdhS2 is likely to
494 affect PleD enzymatic activity through the phosphorylation state of its receiver domain,
495 similar to other PleD homologues (22, 59, 60). Additionally, mutation of *pdhS2*
496 increases *dgcB* transcription providing a direct link to elevated cdGMP production.
497 Whether PdhS2 also regulates DgcA activity remains to be determined.
498
499 **Indirect regulation of CtrA by PdhS2.** A primary candidate for ultimately mediating
500 the effects of PdhS2 on *A. tumefaciens* physiology is the transcriptional regulator CtrA.
501 Our data support altered CtrA activity, and not abundance, as primarily responsible for
502 *pdhS2*- and *divK*-dependent transcriptional responses. There are several examples in
503 *C. crescentus* where altered CtrA activity is observed without apparent significant
504 changes in CtrA abundance (36, 61, 62). There are also several examples in both *C.*
505 *crescentus* and *S. meliloti* where altered PdhS kinase activity results in both perturbed
506 activity and altered abundance of CtrA (39, 63). Our expression analyses suggest that
507 *A. tumefaciens* CtrA functions to both activate some promoters (*e.g.* succinoglycan
508 synthetic genes and *ctrA*) while repressing others (*e.g. dgcB*, Atu3318, and *pdhS1*).
509
510 **Convergence of PdhS2 and VisNR regulatory pathways.** Many phenotypes
511 regulated by PdhS2 mirror those regulated by the LuxR-type transcriptional motility
512 regulators VisR and VisN (50). Loss of either *visN* or *visR* results in strong inhibition of
513 motility and a dramatic increase in attachment and biofilm formation, that is dependent
514 on cdGMP production. Moreover, VisNR effects on attachment require the diguanylate
515 cyclases DgcA and DgcB. Both PdhS2 and VisNR positively regulate succinoglycan

production at the transcriptional level, and negatively regulate transcription of the LuxR-type regulator Atu3318. The promoter region for Atu3318 as well as several of the succinoglycan genes contain a consensus CtrA binding site, and PdhS2 control is most likely mediated through CtrA. It is possible that the increased activity of one or more diguanylate cyclases in the Δ*visR*/Δ*visN* mutants ultimately results in decreased abundance or activity of CtrA. In both *C. crescentus* and *A. tumefaciens*, cdGMP allosterically switches the bifunctional hybrid histidine kinase CckA from kinase to phosphatase mode, downregulating CtrA phosphorylation and DNA-binding activity (30, 31). In contrast, VisNR motility control is mediated directly through transcriptional control of the Rem activator of flagellar gene expression (50, 64). Our *pdhS2* expression profiling does not reveal a decrease in flagellar gene transcription, suggesting distinct mechanisms. Furthermore, the increase in UPP and cellulose production in *visR* and *visN* mutants is cdGMP-dependent, and likely proceeds via allosteric control of the UPP biosynthesis machinery and cellulose synthase (which has a PilZ-type cdGMP binding motif). It is quite plausible that a significant fraction of the *pdhS2* hyper-adherent phenotype reflects similar allosteric control of UPP and cellulose.

Segregation of antagonistic signaling activity promotes asymmetric development. The asymmetric division of *A. tumefaciens* and other Alphaproteobacteria, producing two genetically identical but phenotypically distinct daughter cells, requires well-coordinated regulation of two developmental programs. The mother cell remains in a terminally differentiated state, proceeding through distinct synthesis (S) and growth (G2) phases of the cell cycle (51, 55). During G2 phase the cell elongates into a predivisional

539 cell and establishes a functional asymmetry between its two cellular poles by differential
540 localization of antagonistic homologues of the PdhS kinases. At least one PdhS kinase,
541 DivJ in *C. crescentus* and *A. tumefaciens*, PdhS in *B. abortus* and CbrA in *S. meliloti*,
542 localizes to the attached pole (18, 38) (Fig. 1A and 3B). At this site these kinases can
543 act to phosphorylate DivK and PleD, indirectly inactivating CtrA (as reported for
544 *Caulobacter*). At the opposite pole at least one PdhS kinase, PleC in *C. crescentus* and
545 PdhS2 in *A. tumefaciens* (Fig. 1A and 3A), localizes and acts primarily to
546 dephosphorylate DivK and PleD, ultimately promoting CtrA stability and activity. Upon
547 cytokinesis, then, the motile daughter cell is released in a G1 growth phase with high
548 levels of CtrA activity establishing a distinct transcriptional program.

549 Pole specification may also be generated as a natural consequence of cell
550 division. Following each cytokinetic event a new, younger pole is generated from the
551 division septum. Cell elongation in many Rhizobiales, including *A. tumefaciens*, occurs
552 in the absence of obvious homologues to DivIVA or MreB, important regulators of cell
553 elongation in many rod-shaped bacteria (65). Instead, cell elongation in these bacteria
554 occurs primarily at the younger pole of the bacterium in a process of zonal insertion of
555 peptidoglycan and cell membrane components (6, 7). The canonical cell division
556 proteins FtsZ and FtsA both localize at the growing pole of *A. tumefaciens* until just prior
557 to cytokinesis at which point they relocalize to the cell division septum. Several other *A.*
558 *tumefaciens* proteins, including PopZ and PodJ, act as dynamic fiduciary markers
559 localizing to one or both bacterial poles throughout the cell cycle (66, 67). While these
560 cell cycle, elongation, and division components make use of polar localization the role
561 played by any of these proteins in differentiation of old versus new poles is unclear.

562 Our data are consistent with PdhS2 acting in the motile daughter cell to prevent
563 premature activation of cell attachment processes such as UPP production, as well as
564 to inhibit motility. Our results suggest that Δ*pdhS2* mutant cells are blocked from
565 completely exiting the dividing cell phase and differentiating into the motile cell type.
566 Alternatively, Δ*pdhS2* mutant cells may have an abridged motile cell (G1) phase and
567 prematurely differentiate into the dividing cell type. In either case, *pdhS2* mutants
568 assemble polar flagella in daughter cells, but these seem to be largely blocked for
569 rotation, hence the swimming deficiency in the *pdhS2* mutant.
570 The subtle effects on CtrA abundance coupled with the modest, but significant,
571 effects on several CtrA-dependent promoters, suggest that either PdhS2 regulation of
572 CtrA activity is restricted to a very tight window during the cell cycle or to a specific
573 location within the developing cell Alternatively, the complement of remaining PdhS
574 kinases buffer CtrA activity in the absence of *pdhS2*. Microarray results using
575 unsynchronized cultures of *S. meliloti* lacking either the *divJ* or the *cbrA* PdhS kinase
576 were similar to those in our own study (39, 68). All three datasets uncovered a restricted
577 set of differentially regulated genes, several of which were common to one or more
578 experiment (Table 2). Transcriptional assays of the *dgcB* and Atu3318 promoters are
579 consistent with the microarray data in both directionality and magnitude. It is telling that
580 reporter activity of these potential CtrA-regulated promoters in the Δ*pdhS2* mutant is two
581 to three times higher than the remaining regulated promoters (Table 1). This lower
582 overall activity may explain why more putative CtrA-dependent promoters were not
583 identified in the transcriptional profiling. A reassessment for transcriptional effects of the

584 PdhS kinases will be a high priority once synchronization and cell type enrichment
585 procedures are developed.

586 All of the PdhS-type kinases in *A. tumefaciens* including PleC and DivJ are
587 hypothesized to function through the DivK and PleD response regulators. However, it is
588 clear that they can have starkly distinct regulatory outputs. In *A. tumefaciens pleC* and
589 *pdhS1* mutants manifest defects in budding and form branched cells, whereas the
590 *pdhS2* mutant has no apparent defect in budding, and is instead down for motility and
591 elevated for attachment. These differences may in large measure reflect the spatial and
592 temporal control of their activity. We hypothesize that spatial restriction of PdhS2 activity
593 to the budding poles of mother cells, that rapidly transition to become the old pole of
594 newly formed daughter cells, imparts PdhS2 control of motility and attachment
595 processes, without strongly influencing the budding process *per se*.

596

MATERIALS AND METHODS

Strains and plasmids. Bacterial strains, plasmids, and oligonucleotides used in these studies are listed in Tables S1 through S3. *A. tumefaciens* was routinely cultivated at 28°C in AT minimal medium plus 1% (w/v) glucose as a carbon source and 15 mM $(NH_4)_2SO_4$ as a nitrogen source (ATGN), without exogenous $FeSO_4$ (69, 70). For biofilm assays 22 μM $FeSO_4$ was included in the media. *E. coli* was routinely cultivated at 37°C in lysogeny broth (LB). Antibiotics were used at the following concentrations (*A. tumefaciens*/*E. coli*): ampicillin (100/100 $\mu g \cdot mL^{-1}$), kanamycin (150/25 $\mu g \cdot mL^{-1}$), gentamicin (150/30 $\mu g \cdot mL^{-1}$), spectinomycin (300/100 $\mu g \cdot mL^{-1}$), and tetracycline (4/10 $\mu g \cdot mL^{-1}$).

Non-polar, markerless deletion of *pdhS2* (Atu1888) in all genetic backgrounds used in this work was accomplished using splicing by overlap extension (SOE) polymerase chain reaction (PCR) followed by homologous recombination, as described (35). Suicide plasmid pJEH040 carries an approximately 1 kb SOE deletion fragment of *pdhS2* on a pNPTS138 vector backbone. pNPTS138 is a ColE1 plasmid and as such is unable to replicate in *A. tumefaciens*. pJEH040 was delivered to recipient strains by either transformation or conjugation followed by selection on ATGN plates supplemented with 300 $\mu g \cdot mL^{-1}$ Km, selecting for *A. tumefaciens* cells in which pJEH040 had integrated at the chromosomal *pdhS2* locus by homologous recombination. Recombinants were then grown overnight at 28°C in ATGN in the absence of Km and plated the following day onto ATSN (ATGN with sucrose substituted for glucose) agar plates to select for sucrose resistant (Suc^R) allelic replacement

620 candidates. After three days' growth at 28°C colonies were patched in parallel onto
621 ATGN Km and ATSN plates. Km^S Suc^R recombinants were then tested for the targeted
622 deletion by diagnostic PCR using primers external to the *pdhS2* locus (JEH100 and
623 JEH113) as well as internal primers (JEH85 and JEH87). Candidate colonies were
624 further streak purified and verified a second time by diagnostic PCR before being used
625 in downstream assays.

626 Site-directed mutagenesis of *pdhS2* was achieved using mutagenic primer pairs
627 JEH245/JEH246 (for generating the His271Ala allele, H271A) or JEH261/JEH262 (for
628 generating the Thr275Ala allele, T275A). Plasmid pJEH021 carrying the wild-type
629 *pdhS2* sequence was amplified by PCR using the above primer pairs. Following
630 amplification, reaction mixtures were treated with *Dpn*I restriction endonuclease to
631 remove template plasmid and then transformed into TOP10 F' *E. coli* competent cells.
632 Purified plasmids from each transformation were sequenced and those containing the
633 desired mutations, pJEH091 for His271Ala and pJEH099 for Thr275Ala, were selected
634 for sub-cloning. pJEH091 and pJEH099 were digested with *Nde*I and *Nhe*I followed by
635 gel electrophoresis and purification of the resulting insert. Inserts were ligated into
636 similarly digested pSRKGm and transformed into competent *E. coli* TOP10 F' cells.
637 Purified plasmids from each transformation were sequenced to verify their identity. The
638 resulting plasmids, pJEH092 (H271A) and pJEH102 (T275A), were used to transform *A.*
639 *tumefaciens*. To generate a PdhS2 allele carrying both H271A and T275A mutations the
640 same steps were followed as above using plasmid pJEH091 as template with
641 mutagenic primers JEH261/JEH262.

642 Translational fusions of full-length wild-type PdhS2 and DivJ to GFP were
643 constructed as follows. *pdhS2* and *divJ*, each lacking a stop codon were amplified by
644 PCR using primer pairs JEH65/JEH146 (*pdhS2*) and JEH147/JEH148 (*divJ*) with *A.*
645 *tumefaciens* strain C58 genomic DNA as template. Primer design for these
646 amplifications included 5' *Nde*I and 3' *Nhe*I restriction sites. The *gfpmut3* gene including
647 a 5' *Nhe*I site and a 3' *Kpn*I site was amplified using primer pair JEH149/JEH150 and
648 pJZ383 as template. Amplicons were gel purified, ligated into pGEM-T Easy,
649 transformed into competent TOP10 F' *E. coli*, and eventually sequenced. The resulting
650 plasmids, pJEH052 (*pdhS2*), pJEH053 (*gfpmut3*), and pJEH054 (*divJ*) were digested
651 with either *Nde*I and *Nhe*I (pJEH052 and pJEH054) or *Nhe*I and *Kpn*I (pJEH053).
652 Inserts were gel purified and used in a three-component ligation with *Nde*I/*Kpn*I-
653 digested pSRKGm generating pJEH060 (PdhS2-GFP) and pJEH078 (DivJ-GFP).
654 Sequenced plasmids were used to transform *A. tumefaciens*. Translational fusions of
655 full-length mutant PdhS2 alleles (H271A or T275A) to tdTomato (Table S2) were
656 generated using primers JEH65 and JEH272 with either pJEH091 or pJEH099 as
657 template. The resulting amplicons were gel purified and ligated into pGEM-T Easy to
658 generate plasmids pJEH125 and pJEH126. pJEH125 and pJEH126 were digested with
659 *Nde*I and *Sac*I and the resulting inserts gel purified and ligated with similarly treated
660 pSRKKm-tdTomato, generating plasmids pJEH127 and pJEH128.
661 Reporter gene fusion constructs included predicted promoter regions from
662 between 200 bp and 400 bp upstream of the indicated gene through the start codon.
663 Each upsream region was amplified by PCR using the primers listed in Table S3 using
664 *A. tumefaciens* genomic DNA as template. Amplicons were gel purified, ligated into

665 pGEM-T Easy, transformed into competent TOP10 F' *E. coli*, and eventually
666 sequenced. The resulting plasmids, pJEH113 (*ccrM*, Atu0794, promoter), pJEH115
667 (*ctrA*, Atu2434, promoter), and pJEH119 (*pdhS1*, Atu0614, promoter) were digested
668 with either *Kpn*I and *Hin*DIII (pJEH113 and pJEH119) or *Kpn*I and *Pst*I (pJEH115).
669 Inserts were gel purified and ligated with similarly treated pRA301 containing a
670 promoterless *E. coli lacZ* gene without its own ribosome binding site. The resulting
671 constructs (pJEH121, pJEH122, and pJEH124) carry *lacZ* translationally fused to the
672 start codon for each gene with transcription and translation driven by the fused
673 upstream region. pJEH121, pJEH122, and pJEH124 were used to transform *A.*
674 *tumefaciens* for subsequent beta-galactosidase assays.
675
676 **Static biofilm assays.** Overnight cultures in ATGN were sub-cultured in fresh ATGN to
677 an optical density at 600 nm (OD_{600}) of 0.1 and grown with aeration at 28°C until an
678 OD_{600} of 0.25-0.6. Cultures were diluted to OD_{600} of 0.05 and 3 mL were inoculated into
679 each of four wells in a 12-well plate. A single coverslip was placed vertically into each
680 well to submerge approximately half of each coverslip. Plates were incubated in a
681 humidified chamber at 28° for 48 h. Coverslips were removed from each well, rinsed
682 with water, and adherent biomass stained by 5 min immersion in a 0.1% (w/v) crystal
683 violet solution. Adsorbed crystal violet was solubilized by immersion in 1 mL 33% acetic
684 acid and the absorbance of this solution determined at 600 nm (A_{600}) on a Synergy HT
685 multi-detection microplate reader (Bio-Tek). Culture density for each sample was also
686 determined by measuring the OD_{600} of each culture. Data are typically presented as
687 A_{600}/OD_{600} ratios normalized to values obtained for the wild-type strain within each

688 experiment. ATGN was supplemented with antibiotics and IPTG as appropriate. Final
689 inoculations also included supplemental iron (22 μM). Each mutant was evaluated in
690 three independent experiments each of which contained three technical replicates.
691
692 **Motility assays.** Wet mounts of exponentially growing cultures were observed under
693 brightfield optics using a Zeiss Axioskop 40 equipped with an AxioCam MRm
694 monochrome digital camera. Swim plates containing 0.3% agarose in ATGN,
695 supplemented with 1 mM IPTG and antibiotics when appropriate, were inoculated with a
696 single colony of the indicated strain at a central point and incubated for 7 days at 28°C.
697 Swim ring diameters were measured daily for seven days. Each experimental condition
698 was tested in three independent experiments containing three technical replicates.
699
700 **Microscopy.** Cell morphology and localization of PdhS2-GFP and DivJ-GFP was
701 evaluated using a Nikon E800 fluorescence microscope equipped with a Photometrics
702 Cascade cooled CCD camera. Overnight cultures were grown in ATGN with gentamicin
703 and 250 μM IPTG. The following day each strain was sub-cultured to OD_{600} 0.1 and
704 then grown at 28°C with aeration until ~OD_{600} 0.5-0.8. The culture (0.5 μl) was
705 transferred to a 1% ATGN/agarose pad on a clean glass slide and a clean 22 x 22 mm
706 number 1.5 glass coverslip placed on top. Images were acquired using a 100X oil
707 immersion objective and phase contrast optics or epifluorescence with a FITC-HYQ
708 filter set (Nikon; excitation filter = 480/40 nm, dichromatic mirror = 505 nm, absorption
709 filter = 535/50 nm). Time-lapse microscopy utilized a Nikon Ti-E inverted fluorescence
710 microscope with a Plan Apo 60X/1.40 oil Ph3 DM objective, a DAPI/FITC/Cy3/Cy5 filter

711 cube, an Andor iXon3 885 EMCCD camera, and a Lumencor Spectra X solid state light
712 engine at 20% power. For time-lapse imaging agarose pads included 250 μM IPTG and
713 coverslips were attached to the glass slide using a gas-permeable 1:1:1 mixture of
714 Vaseline, lanolin, and paraffin. Phase and fluorescence images were captured every 20
715 min for 8 h using a 60 ms (phase) or 2 s (fluorescence) exposure. Images were
716 analyzed using ImageJ (Schneider *et al.*, 2012, Schindelin *et al.*, 2012, Schindelin *et al.*,
717 2015). Localization of all PdhS2-tdTomato constructs was evaluated using a Zeiss
718 AxioObserver.Z1 fluorescence microscope equipped with a Photometrics Cascade
719 cooled CCD camera. Cultures were treated as above and images acquired using a 100x
720 oil immersion objective and Semrock TXRED-4040b-zhe-zero filter cube.
721
722 **Transcriptional profiling.** Whole-genome transcriptional profiling using custom 60-
723 mer oligonucleotide microarrays was performed essentially as previously described
724 (71). Arrays were produced by Agilent Technologies, and consist of 8455 features that
725 represent 5338 predicted protein-encoding open reading frames, tRNA and rRNA
726 encoding genes, and 2,983 duplicate spots. Cultures of wild-type or the Δ*pdhS2* mutant
727 strain of *A. tumefaciens* strain C58 were grown overnight in ATGN to full turbidity and
728 then sub-cultured 1:150 into fresh ATGN for a second overnight growth. The following
729 morning a volume equivalent to 11 ml of OD_{600} 0.6 was prepared for RNA extraction
730 using RNAprotect Bacteria Reagent (QIAGEN, Germantown, MD) following the
731 manufacturer's protocol. RNA was extracted from these samples using QIAGEN RNA
732 midipreps (QIAGEN, Germantown, MD) following the manufacturer's protocol. DNA
733 contamination was removed by DNase digestion using the TURBO DNA-free kit

(Ambion, Austin, TX) with the incubation time extended to two hours. First strand cDNA synthesis was performed using Invitrogen SuperScript Indirect Labeling Kit, and cDNA was purified on Qiagen QIAQuick columns. cDNA was labeled with AlexaFluor 555 and 647 dyes using Invitrogen SuperScript cDNA Labeling Kit, and repurified on QIAQuick columns. cDNA was quantified on a NanoDrop spectrophotometer. Hybridization reactions were performed using Agilent in situ Hybridization Kit Plus, boiled for 5 min at 95°C, applied to the printed arrays, and hybridized overnight at 65°C. Hybridized arrays were washed with Agilent Wash Solutions 1 and 2, rinsed with acetonitrile, and incubated in Agilent Stabilization and Drying Solution immediately prior to scanning the arrays. Three independent biological replicates were performed, with one dye swap. Hybridized arrays were scanned on a GenePix Scanner 4200 in the Center for Genomics and Bioinformatics (CGB) at Indiana University. GenePix software was used to define the borders of hybridized spots, subtract background, measure dye intensity at each spot, and calculate the ratio of dye intensities for each spot. Analysis of the scanned images was conducted using the LIMMA package in R/Bioconductor. Background correction of the data was performed using the minimum method (72, 73). The data was normalized within arrays with the LOESS method, and between arrays with the quantile method. Statistical analysis was performed using linear model fitting and empirical Bayesian analysis by least squares. Genes with significant *P* values (≤ 0.05) and with $\log_2$ ratios of ≥ 0.50 or ≤ -0.50 (representing a fold-change of ± 1.4) are reported here. Expression data have been deposited in the Gene Expression Omnibus (GEO) database at the National Center for Biotechnology Information (NCBI) under accession number GSE71267 (74).

757 β-galactosidase activity was measured using a modified protocol of Miller (75).
758 Cultures carrying transcriptional reporter plasmids were grown overnight in ATGN and
759 sub-cultured the following morning to OD_{600} 0.15. Diluted cultures were grown at 28°C
760 with aeration until reaching mid-exponential growth. Between 100 and 300 μL of
761 exponential phase culture was mixed with Z buffer (60 mM Na_2HPO_4, 40 mM NaH_2PO_4,
762 10 mM KCl, 1 mM $MgSO_4$, pH = 7.0) to a final volume of 1 mL (volume of culture = f)
763 plus two drops 0.05% sodium dodecyl sulfate and 3 drops $CHCl_3$. The amount of culture
764 volume used was calibrated to generate reaction times between 15 minutes and two
765 hours for cultures with activity. 0.1 mL of a 4 $mg \cdot mL^{-1}$ solution in Z buffer of the
766 colorimetric substrate 2-nitrophenyl β-D-galactopyranoside (ONPG) was added and the
767 time (t) required for the solution to turn yellow was recorded. The reaction was stopped
768 by addition of 1 M Na_2CO_3 and the absorbance at 420 nm (A_{420}) of each solution was
769 measured. Promoter activity is expressed in Miller units (MUs = [1000 x A_{420nm}]/[OD_{600nm}
770 x t x f]). Each mutant was tested in three independent experiments containing five
771 technical replicates.
772
773 **Protein stability assays.** Steady-state levels of CtrA were determined from stationary
774 phase cultures of wild-type, Δ*divK*, and Δ*pdhS2* strains of *A. tumefaciens*. Overnight
775 cultures of each strain were grown in TY broth at 28ºC with aeration to an OD_{600} > 1.
776 Two 1 mL aliquots were removed from each culture, pelleted by centrifugation (13,200 x
777 *g*, 2 min) and supernatants discarded. One of the resulting pellets was resuspended on
778 ice in 50 μL 100 mM Tris·HCl, pH 6.8, followed by 50 μL 2X SDS-PAGE loading buffer
779 (65.8 mM Tris·HCl, pH 6.8, 26.3% (v/v) glycerol, 2.1% (w/v) sodium dodecyl sulfate

780 (SDS), 0.01% (w/v) bromophenol blue), then stored frozen at -20ºC. The second pellet
781 was resuspended in 100 μL 1X protein assay buffer (32.9 mM Tris·HCl, pH 6.8,
782 1%SDS), boiled 10 minutes, and used for protein concentration determination using the
783 Pierce BCA Protein Assay Kit (Thermo Fisher Scientific), per manufacturer's
784 instructions. Frozen resuspended pellets were thawed on ice and β-mercaptoethanol
785 added to a final concentration of 5% prior to electrophoresis. Samples were normalized
786 for protein concentration and separated on a 12.5% SDS-polyacrylamide gel. Following
787 electrophoresis proteins were transferred to Immobilon-FL polyvinyl difluoride
788 membranes (EMD Millipore). Membranes were rinsed in 1X Tris-buffered saline (TBS;
789 50 mM Tris·HCl, pH 7.5, 150 mM NaCl) solution and air dried. Membranes were wetted
790 with MeOH and incubated in blocking buffer (1X TBS, 5% non-fat dairy milk [NFDM]) for
791 1 h at room temperature and then incubated overnight at 4ºC with primary antibody
792 (1:5000 dilution of rabbit anti-CtrA from *C. crescentus,* anti-$CtrA_{Cc}$, in 1X TBS/5%
793 NFDM/0.2% Tween 20). The following day membranes were rinsed thoroughly with 1X
794 TBS/0.1% Tween 20 and incubated 1 h at room temperature with secondary antibody
795 (1:20,000 dilution of IRDye 800CW-conjugated goat anti-rabbit antibody (LI-COR) in 1X
796 TBS/5% NFDM/0.2% Tween 20/0.01% SDS). Membranes were rinsed thoroughly with
797 1X TBS/0.1% Tween 20 followed by 1X TBS alone and air dried in the dark. The
798 resulting blot was imaged using a LI-COR Odyssey Classic infrared imaging system.
799 Band intensities were quantified using the Odyssey Classic software.

800 Proteolytic turnover of CtrA was evaluated using translational shut-off assays.
801 Overnight cultures were grown in TY broth at 28ºC with aeration. The following day
802 each strain was sub-cultured in fresh TY broth to an OD_{600} 0.05 and incubated at 28ºC

with aeration. To inhibit protein synthesis 90 μg·mL^{-1} chloramphenicol was added to each culture at OD_{600} 0.5. Starting at the time of chloramphenicol addition 5 mL aliquots were removed every 30 min for 3 h. Each aliquot was pelleted by centrifugation (5000 x *g*, 10 min). Cleared supernatants were discarded and pellets resuspended to an OD_{600} 10.0 in Tris-Cl, (10 mM, pH 8.0). Resuspended pellets were mixed with 2X SDS-PAGE loading buffer and stored frozen at -20ºC. Levels of CtrA were determined by SDS-PAGE and Western blotting as described above. Band intensities were quantified using the Odyssey Classic software and normalized to the band intensity of CtrA from the wild-type background at t = 0 min.

Global cdGMP measurement. Measurement of cdGMP levels was performed by liquid chromatography, tandem mass spectrometry (LC-MS/MS) on a Quattro Premier XE mass spectrometer coupled with an Acquity Ultra Performance LC system (Waters Corporation), essentially as previously described (76). Concentrations of cdGMP in cell samples were compared to chemically synthesized cdGMP (Axxora) dissolved in water at concentrations of 250, 125, 62.5, 31.2, 15.6, 7.8, 3.9, and 1.9 nM to generate a calibration curve. *A. tumefaciens* derivatives were grown in ATGN overnight at 28ºC to stationary phase. Culture densities were normalized after collecting cells by centrifugation and then resuspension in the appropriate volume of ATGN. Cultures were then pelleted by centrifugation and resuspended in ice-cold 250 μL extraction buffer (methanol:acetonitrile:water, 40:40:20 + 0.1 N formic acid) and incubated for 30 min at -20ºC. Resuspensions were transferred to microcentrifuge tubes and pelleted (13,000 x rpm, 5 min). 200 μL of the resulting supernatant was neutralized with 8 μL 15%

826 NH_4HCO_3. Neutralized samples were stored at -20ºC prior to mass spectrometry

827 analysis.

828

829 ## ACKNOWLEDGEMENTS

830 This project was supported by National Institutes of Health (NIH) grants GM080546
831 (C.F.) and GM109259 (C.M.W.). J.E.H. was supported by a Ruth L. Kirschstein National
832 Research Service Award (1 F32 GM100601) from the NIH.

833

REFERENCES

1. **Kysela DT, Randich AM, Caccamo PD, Brun YV**. 2016. Diversity takes shape: understanding the mechanistic and adaptive basis of bacterial morphology. PLoS Biol **14**:e1002565.
2. **Dworkin M**. 1985. Developmental biology of the bacteria. Benjamin/Cummings Pub. Co., Reading, Mass.
3. **Hajduk IV, Rodrigues CD, Harry EJ**. 2016. Connecting the dots of the bacterial cell cycle: Coordinating chromosome replication and segregation with cell division. Semin Cell Dev Biol **53**:2-9.
4. **Costerton JW, Lewandowski Z, Caldwell DE, Korber DR, Lappin-Scott HM**. 1995. Microbial biofilms. Annu Rev Microbiol **49**:711-45.
5. **Jonas K**. 2014. To divide or not to divide: control of the bacterial cell cycle by environmental cues. Curr Opin Microbiol **18**:54-60.
6. **Brown PJ, de Pedro MA, Kysela DT, Van der Henst C, Kim J, De Bolle X, Fuqua C, Brun YV**. 2012. Polar growth in the Alphaproteobacterial order Rhizobiales. Proc Natl Acad Sci U S A **109**:1697-701.
7. **Zupan JR, Cameron TA, Anderson-Furgeson J, Zambryski PC**. 2013. Dynamic FtsA and FtsZ localization and outer membrane alterations during polar growth and cell division in *Agrobacterium tumefaciens*. Proc Natl Acad Sci U S A **110**:9060-5.
8. **Reuter SH, Shapiro L**. 1987. Asymmetric segregation of heat-shock proteins upon cell division in *Caulobacter crescentus*. J Mol Biol **194**:653-62.
9. **Lindner AB, Madden R, Demarez A, Stewart EJ, Taddei F**. 2008. Asymmetric segregation of protein aggregates is associated with cellular aging and rejuvenation. Proc Natl Acad Sci U S A **105**:3076-81.
10. **Kysela DT, Brown PJ, Huang KC, Brun YV**. 2013. Biological consequences and advantages of asymmetric bacterial growth. Annu Rev Microbiol **67**:417-35.
11. **Berne C, Ma X, Licata NA, Neves BR, Setayeshgar S, Brun YV, Dragnea B**. 2013. Physiochemical properties of *Caulobacter crescentus* holdfast: a localized bacterial adhesive. J Phys Chem B **117**:10492-503.
12. **Curtis PD, Brun YV**. 2010. Getting in the loop: regulation of development in *Caulobacter crescentus*. Microbiol Mol Biol Rev **74**:13-41.
13. **Quon KC, Marczynski GT, Shapiro L**. 1996. Cell cycle control by an essential bacterial two-component signal transduction protein. Cell **84**:83-93.
14. **Domian IJ, Reisenauer A, Shapiro L**. 1999. Feedback control of a master bacterial cell-cycle regulator. Proc Natl Acad Sci U S A **96**:6648-53.
15. **Lasker K, Mann TH, Shapiro L**. 2016. An intracellular compass spatially coordinates cell cycle modules in *Caulobacter crescentus*. Curr Opin Microbiol **33**:131-139.
16. **Jenal U, Fuchs T**. 1998. An essential protease involved in bacterial cell-cycle control. EMBO J **17**:5658-69.
17. **Siam R, Marczynski GT**. 2000. Cell cycle regulator phosphorylation stimulates two distinct modes of binding at a chromosome replication origin. EMBO J **19**:1138-47.
18. **Wheeler RT, Shapiro L**. 1999. Differential localization of two histidine kinases controlling bacterial cell differentiation. Mol Cell **4**:683-94.
19. **Viollier PH, Sternheim N, Shapiro L**. 2002. Identification of a localization factor for the polar positioning of bacterial structural and regulatory proteins. Proc Natl Acad Sci U S A **99**:13831-6.

20. **Hinz AJ, Larson DE, Smith CS, Brun YV**. 2003. The *Caulobacter crescentus* polar organelle development protein PodJ is differentially localized and is required for polar targeting of the PleC development regulator. Mol Microbiol **47**:929-41.
21. **Radhakrishnan SK, Thanbichler M, Viollier PH**. 2008. The dynamic interplay between a cell fate determinant and a lysozyme homolog drives the asymmetric division cycle of *Caulobacter crescentus*. Genes Dev **22**:212-25.
22. **Paul R, Jaeger T, Abel S, Wiederkehr I, Folcher M, Biondi EG, Laub MT, Jenal U**. 2008. Allosteric regulation of histidine kinases by their cognate response regulator determines cell fate. Cell **133**:452-61.
23. **Tropini C, Huang KC**. 2012. Interplay between the localization and kinetics of phosphorylation in flagellar pole development of the bacterium *Caulobacter crescentus*. PLoS Comput Biol **8**:e1002602.
24. **Subramanian K, Paul MR, Tyson JJ**. 2013. Potential role of a bistable histidine kinase switch in the asymmetric division cycle of *Caulobacter crescentus*. PLoS Comput Biol **9**:e1003221.
25. **Subramanian K, Paul MR, Tyson JJ**. 2015. Dynamical localization of DivL and PleC in the asymmetric division cycle of *Caulobacter crescentus*: A theoretical investigation of alternative models. PLoS Comput Biol **11**:e1004348.
26. **Quon KC, Yang B, Domian IJ, Shapiro L, Marczynski GT**. 1998. Negative control of bacterial DNA replication by a cell cycle regulatory protein that binds at the chromosome origin. Proc Natl Acad Sci U S A **95**:120-5.
27. **Laub MT, Chen SL, Shapiro L, McAdams HH**. 2002. Genes directly controlled by CtrA, a master regulator of the *Caulobacter* cell cycle. Proc Natl Acad Sci U S A **99**:4632-7.
28. **Laub MT, McAdams HH, Feldblyum T, Fraser CM, Shapiro L**. 2000. Global analysis of the genetic network controlling a bacterial cell cycle. Science **290**:2144-8.
29. **Chen YE, Tsokos CG, Biondi EG, Perchuk BS, Laub MT**. 2009. Dynamics of two phosphorelays controlling cell cycle progression in *Caulobacter crescentus*. J Bacteriol **191**:7417-29.
30. **Dubey BN, Lori C, Ozaki S, Fucile G, Plaza-Menacho I, Jenal U, Schirmer T**. 2016. Cyclic di-GMP mediates a histidine kinase/phosphatase switch by noncovalent domain cross-linking. Sci Adv **2**:e1600823.
31. **Lori C, Ozaki S, Steiner S, Bohm R, Abel S, Dubey BN, Schirmer T, Hiller S, Jenal U**. 2015. Cyclic di-GMP acts as a cell cycle oscillator to drive chromosome replication. Nature **523**:236-9.
32. **Tsokos CG, Perchuk BS, Laub MT**. 2011. A dynamic complex of signaling proteins uses polar localization to regulate cell-fate asymmetry in Caulobacter crescentus. Dev Cell **20**:329-41.
33. **Childers WS, Xu Q, Mann TH, Mathews, II, Blair JA, Deacon AM, Shapiro L**. 2014. Cell fate regulation governed by a repurposed bacterial histidine kinase. PLoS Biol **12**:e1001979.
34. **Chen YE, Tropini C, Jonas K, Tsokos CG, Huang KC, Laub MT**. 2011. Spatial gradient of protein phosphorylation underlies replicative asymmetry in a bacterium. Proc Natl Acad Sci U S A **108**:1052-7.
35. **Kim J, Heindl JE, Fuqua C**. 2013. Coordination of division and development influences complex multicellular behavior in *Agrobacterium tumefaciens*. PLoS One **8**:e56682.
36. **Curtis PD, Brun YV**. 2014. Identification of essential alphaproteobacterial genes reveals operational variability in conserved developmental and cell cycle systems. Mol Microbiol **93**:713-35.
37. **Romling U, Galperin MY, Gomelsky M**. 2013. Cyclic di-GMP: the first 25 years of a universal bacterial second messenger. Microbiol Mol Biol Rev **77**:1-52.
38. **Hallez R, Bellefontaine AF, Letesson JJ, De Bolle X**. 2004. Morphological and functional asymmetry in alpha-proteobacteria. Trends Microbiol **12**:361-5.

39. **Pini F, Frage B, Ferri L, De Nisco NJ, Mohapatra SS, Taddei L, Fioravanti A, Dewitte F, Galardini M, Brilli M, Villeret V, Bazzicalupo M, Mengoni A, Walker GC, Becker A, Biondi EG**. 2013. The DivJ, CbrA and PleC system controls DivK phosphorylation and symbiosis in *Sinorhizobium meliloti*. Mol Microbiol **90**:54-71.
40. **Gao R, Stock AM**. 2009. Biological insights from structures of two-component proteins. Annu Rev Microbiol **63**:133-54.
41. **Huynh TN, Stewart V**. 2011. Negative control in two-component signal transduction by transmitter phosphatase activity. Mol Microbiol **82**:275-86.
42. **Tsokos CG, Laub MT**. 2012. Polarity and cell fate asymmetry in *Caulobacter crescentus*. Curr Opin Microbiol **15**:744-50.
43. **Laloux G, Jacobs-Wagner C**. 2014. How do bacteria localize proteins to the cell pole? J Cell Sci **127**:11-9.
44. **Hallez R, Mignolet J, Van Mullem V, Wery M, Vandenhaute J, Letesson JJ, Jacobs-Wagner C, De Bolle X**. 2007. The asymmetric distribution of the essential histidine kinase PdhS indicates a differentiation event in *Brucella abortus*. EMBO J **26**:1444-55.
45. **Lam H, Matroule JY, Jacobs-Wagner C**. 2003. The asymmetric spatial distribution of bacterial signal transduction proteins coordinates cell cycle events. Dev Cell **5**:149-59.
46. **Kahng LS, Shapiro L**. 2001. The CcrM DNA methyltransferase of *Agrobacterium tumefaciens* is essential, and its activity is cell cycle regulated. J Bacteriol **183**:3065-75.
47. **Brilli M, Fondi M, Fani R, Mengoni A, Ferri L, Bazzicalupo M, Biondi EG**. 2010. The diversity and evolution of cell cycle regulation in alpha-proteobacteria: a comparative genomic analysis. BMC Syst Biol **4**:52.
48. **Skerker JM, Shapiro L**. 2000. Identification and cell cycle control of a novel pilus system in *Caulobacter crescentus*. EMBO J **19**:3223-34.
49. **Stephens CM, Zweiger G, Shapiro L**. 1995. Coordinate cell cycle control of a Caulobacter DNA methyltransferase and the flagellar genetic hierarchy. J Bacteriol **177**:1662-9.
50. **Xu J, Kim J, Koestler BJ, Choi JH, Waters CM, Fuqua C**. 2013. Genetic analysis of *Agrobacterium tumefaciens* unipolar polysaccharide production reveals complex integrated control of the motile-to-sessile switch. Mol Microbiol **89**:929-48.
51. **Heindl JE, Wang Y, Heckel BC, Mohari B, Feirer N, Fuqua C**. 2014. Mechanisms and regulation of surface interactions and biofilm formation in *Agrobacterium*. Front Plant Sci **5**:176.
52. **Douglas CJ, Staneloni RJ, Rubin RA, Nester EW**. 1985. Identification and genetic analysis of an Agrobacterium tumefaciens chromosomal virulence region. J Bacteriol **161**:850-60.
53. **Skerker JM, Laub MT**. 2004. Cell-cycle progression and the generation of asymmetry in *Caulobacter crescentus*. Nat Rev Microbiol **2**:325-37.
54. **Sadowski CS, Wilson D, Schallies KB, Walker G, Gibson KE**. 2013. The *Sinorhizobium meliloti* sensor histidine kinase CbrA contributes to free-living cell cycle regulation. Microbiology **159**:1552-63.
55. **Panis G, Murray SR, Viollier PH**. 2015. Versatility of global transcriptional regulators in alpha-Proteobacteria: from essential cell cycle control to ancillary functions. FEMS Microbiol Rev **39**:120-33.
56. **De Bolle X, Crosson S, Matroule JY, Letesson JJ**. 2015. *Brucella abortus* cell cycle and infection are coordinated. Trends Microbiol **23**:812-21.
57. **Quinones-Valles C, Sanchez-Osorio I, Martinez-Antonio A**. 2014. Dynamical modeling of the cell cycle and cell fate emergence in *Caulobacter crescentus*. PLoS One **9**:e111116.
58. **Fields AT, Navarrete CS, Zare AZ, Huang Z, Mostafavi M, Lewis JC, Rezaeihaghighi Y, Brezler BJ, Ray S, Rizzacasa AL, Barnett MJ, Long SR, Chen EJ, Chen JC**. 2012. The conserved polarity factor

podJ1 impacts multiple cell envelope-associated functions in *Sinorhizobium meliloti*. Mol Microbiol **84**:892-920.

59. **Aldridge P, Paul R, Goymer P, Rainey P, Jenal U**. 2003. Role of the GGDEF regulator PleD in polar development of *Caulobacter crescentus*. Mol Microbiol **47**:1695-708.
60. **Lai TH, Kumagai Y, Hyodo M, Hayakawa Y, Rikihisa Y**. 2009. The *Anaplasma phagocytophilum* PleC histidine kinase and PleD diguanylate cyclase two-component system and role of cyclic di-GMP in host cell infection. J Bacteriol **191**:693-700.
61. **Radhakrishnan SK, Pritchard S, Viollier PH**. 2010. Coupling prokaryotic cell fate and division control with a bifunctional and oscillating oxidoreductase homolog. Dev Cell **18**:90-101.
62. **Pierce DL, O'Donnol DS, Allen RC, Javens JW, Quardokus EM, Brun YV**. 2006. Mutations in DivL and CckA rescue a divJ null mutant of *Caulobacter crescentus* by reducing the activity of CtrA. J Bacteriol **188**:2473-82.
63. **Schallies KB, Sadowski C, Meng J, Chien P, Gibson KE**. 2015. *Sinorhizobium meliloti* CtrA Stability Is Regulated in a CbrA-Dependent Manner That Is Influenced by CpdR1. J Bacteriol **197**:2139-49.
64. **Rotter C, Muhlbacher S, Salamon D, Schmitt R, Scharf B**. 2006. Rem, a new transcriptional activator of motility and chemotaxis in *Sinorhizobium meliloti*. J Bacteriol **188**:6932-42.
65. **Margolin W**. 2009. Sculpting the bacterial cell. Curr Biol **19**:R812-22.
66. **Anderson-Furgeson JC, Zupan JR, Grangeon R, Zambryski PC**. 2016. Loss of PodJ in *Agrobacterium tumefaciens* leads to ectopic polar growth, branching, and reduced cell division. J Bacteriol doi:10.1128/JB.00198-16.
67. **Grangeon R, Zupan JR, Anderson-Furgeson J, Zambryski PC**. 2015. PopZ identifies the new pole, and PodJ identifies the old pole during polar growth in *Agrobacterium tumefaciens*. Proc Natl Acad Sci U S A **112**:11666-71.
68. **Gibson KE, Barnett MJ, Toman CJ, Long SR, Walker GC**. 2007. The symbiosis regulator CbrA modulates a complex regulatory network affecting the flagellar apparatus and cell envelope proteins. J Bacteriol **189**:3591-602.
69. **Tempe J, Petit A, Holsters M, Montagu MV, Schell J**. 1977. Thermosensitive step associated with transfer of Ti plasmid during conjugation - possible relation to transformation in crown gall. Proceedings of the National Academy of Sciences of the United States of America **74**:2848-2849.
70. **Morton ER, Fuqua C**. 2012. Laboratory maintenance of *Agrobacterium*. Curr Protoc Microbiol **Chapter 1**:Unit3D 1.
71. **Heindl JE, Hibbing ME, Xu J, Natarajan R, Buechlein AM, Fuqua C**. 2015. Discrete responses to limitation for iron and manganese in *Agrobacterium tumefaciens*: Influence on attachment and biofilm formation. J Bacteriol **198**:816-29.
72. **Ritchie ME, Phipson B, Wu D, Hu Y, Law CW, Shi W, Smyth GK**. 2015. limma powers differential expression analyses for RNA-sequencing and microarray studies. Nucleic Acids Res **43**:e47.
73. R Core Team. 2016. R: A language and environment for statistical computing., *on* R Foundation for Statistical Computing. https://www.R-project.org. Accessed
74. **Edgar R, Domrachev M, Lash AE**. 2002. Gene Expression Omnibus: NCBI gene expression and hybridization array data repository. Nucleic Acids Res **30**:207-10.
75. **Miller JH**. 1972. Experiments in Molecular Genetics. Cold Spring Harbor, New York.
76. **Wang Y, Kim SH, Natarajan R, Heindl JE, Bruger EL, Waters CM, Michael AJ, Fuqua C**. 2016. Spermidine inversely influences surface interactions and planktonic growth in *Agrobacterium tumefaciens*. J Bacteriol **198**:2682-91.

Tables

Table 1. Promoter activity of selected known and predicted CtrA-dependent promoters.[a]

Strain	Promoter source organism	Promoter	Activity (%WT ± SE)
WT	*C. crescentus*	*ccrM*	100 ± 1
		ctrA	100 ± 2
		pilA	100 ± 1
	A. tumefaciens	*ccrM*	100 ± 1
		ctrA	101 ± 1
		pdhS1	100 ± 1
		dgcB	100 ± 12
		Atu3318	104 ± 25
Δ*pdhS2*	*C. crescentus*	*ccrM*	109 ± 12
		ctrA	82 ± 4 [b]
		pilA	85 ± 2 [b]
	A. tumefaciens	*ccrM*	106 ± 2 [b]
		ctrA	84 ± 3 [b]
		pdhS1	119 ± 3 [b]
		dgcB	201 ± 26 [b]
		Atu3318	352 ± 13 [b]
Δ*divK*	*C. crescentus*	*ccrM*	140 ± 6 [b]
		ctrA	132 ± 4 [b]
		pilA	99 ± 3
	A. tumefaciens	*ccrM*	116 ± 3 [b]
		ctrA	117 ± 2 [b]
		pdhS1	90 ± 1 [b]
		dgcB	N.D. [c]
		Atu3318	N.D. [c]

[a] Promoter activity was measured as β-galactosidase activity of cell lysates from strains carrying either transcriptional (for *C. crescentus* promoters) or translational (for *A. tumefaciens* promoters) fusions of the indicated promoter regions to the *E. coli lacZ* gene. Activity for each promoter was normalized to activity in lysates from wild-type cells carrying the identical promoter. N = 9.

1028

1029 [b] $P < 0.05$ compared to WT value using Student's *t* test.

1030

1031 [c] N.D., not determined.

1032

1033 **Table 2. Differentially-regulated genes in the absence of *pdhS2*.[a]**

Locus ID	Gene	Product[b]	log_2 FC	CtrA site?[c]	Present in other PdhS arrays?[d]
Atu0461	-	*phage tail protein/type VI secretion system component*	2.42	yes	no
Atu0227	-	tRNA-Leu	2.15	no	no
Atu5167	*avhB6*	type IV secretion protein	2.01	no	no
Atu2490	*asd*	aspartate semialdehyde dehydrogenase	1.93	no	no
Atu3318	-	LuxR family transcriptional regulator	1.84	yes	no
Atu1471	*rluC*	ribosomal large subunit pseudouridine synthase C	1.84	no	no
Atu3755	*purK*	phosphoribosylaminoimidazole carboxylase ATPase subunit	1.70	no	no
Atu3606	*ftsE*	cell division ATP-binding protein	1.63	no	no
Atu1791	-	ABC transporter, membrane spanning protein (sugar)	1.55	yes	no
Atu3572	-	XRE family transcriptional regulator	1.52	no	yes
Atu2217	-	*hypothetical protein*	1.52	no	no
Atu5119	*phoB*	two component response regulator	1.48	no	no
Atu3031	-	*hypothetical protein*	1.46	no	no
Atu1886	-	*DNA glycosylase*	1.41	no	no
Atu1964	-	tRNA-Trp	1.40	no	no
Atu1301	-	*Nudix hydrolase*	1.39	no	no
Atu3610	-	cation transporter	1.34	no	no
Atu6048	-	*RNA helicase*	1.32	no	no
Atu1691	*dgcB*	GGDEF family protein	1.32	yes	no
Atu1887	*exoI*	succinoglycan biosynthesis protein	1.30	no	no
Atu1134	-	*lysyl-phosphatidylglycerol synthase*	1.30	no	no
Atu2665	-	MarR family transcriptional regulator	1.27	no	no
Atu2204	-	*hypothetical protein*	1.25	yes	no
Atu0540	-	*hypothetical protein*	1.25	no	no
Atu4856	-	nucleotidyltransferase	-1.21	no	no
Atu4347	*tae*	type VI secreted effector	-1.23	yes	no
Atu4055	*exoK*	endo-1,3-1,4-beta-glycanase	-1.28	yes	yes
Atu4345	*tssD*	type VI secretion needle tube protein	-1.29	yes	no
Atu5091	*rcdB*	curdlan synthesis protein	-1.32	yes	no
Atu4357	-	*transglutaminase-like Cys protease*	-1.34	no	yes
Atu0343	*barA*	two component sensor kinase/response regulator hybrid	-1.37	no	no
Atu4053	*exoA*	succinoglycan biosynthesis protein	-1.42	yes	yes
Atu4056	*exoH*	succinoglycan biosynthesis protein	-1.42	yes	yes
Atu3564	*exsH*	endo-1,3-1,4-beta-glycanase	-1.46	no	no
Atu3541	-	*transglutaminase-like Cys protease*	-1.51	no	no

Atu4627	-	*hypothetical protein*	-1.56	no	no
Atu4049	*exoP*	exopolysaccharide polymerization/transport protein	-1.64	no	no
Atu1469	-	hypothetical protein	-1.80	yes	no
Atu4050	*exoN*	UTP-glucose-1-phosphate uridylyltransferase	-1.82	no	yes

[a] Gene expression was compared between WT and Δ*pdhS2* strains using whole-genome microarrays. Genes were defined as differentially regulated when the following conditions were met: $\log_2$ FC ≥ 0.50 OR $\log_2$ FC ≤ -0.50, AND $P < 0.050$, AND Q < 0.10.

[b] Predicted functions of hypothetical proteins, if available, are italicized.

[c] 500 nt upstream and 100 nt downstream of start codon for each gene (or operon, if applicable) was scanned for possible CtrA binding sites, as described in the text.

[d] Results were compared with previously published *S. meliloti cbrA* and *divJ* microarrays and *C. crescentus divJ* and *pleC* microarrays, as described in the text.

Figure Legends

Figure 1. The PdhS kinases of *C. crescentus* and *A. tumefaciens* differentially localize and affect phenotypic outputs through response regulators DivK, PleD, and CtrA. (A) Cartoon model of known localization of the namesake PdhS kinases from *C. crescentus*, PleC and DivJ, and two PdhS kinases from *A. tumefaciens*, PdhS2 and DivJ. Kinases represented as colored ovals with black border experimentally localize to the indicated poles. Ovals without border have not been experimentally demonstrated to localize. As a result of this localization phosphorylation status of direct PdhS kinase targets, DivK and PleD, and the indirect target, CtrA, is differentially affected. (B) Multiple sequence alignment of the HisKA domain from the PdhS kinases of *C. crescentus* and *A. tumefaciens*. Sequences were aligned using the Clustal Omega web service hosted by the European Molecular Biology Laboratory (EMBL)-European Bioinformatics Institute. The four PdhS kinases from *A. tumefaciens* plus PleC and DivJ from *C. crescentus* were included. Also included are two additional predicted PdhS kinases, CC_0652 and CC_1062, from *C. crescentus*. The EnvZ sensor kinase is included for comparison. Yellow highlighting indicates defining residues for the PdhS kinases. The conserved histidine and threonine residues mutated in this work are in bold. (C) Domain architecture of PdhS2 and DivJ from *A. tumefaciens* as determined using the Simple Modular Architecture Research Tool hosted by EMBL. The C-terminal HisKA and HATPase_c domains are labeled. Blue bars represent predicted transmembrane domains. Purple dashes indicate low complexity domains.

Figure 2. PdhS2 lies upstream of DivK and is predominated by phosphatase activity. (A) Static biofilm formation after 48 h (black bars) and swim ring diameter after 7 days (white bars) of the indicated wild-type and mutant strains. Adherent biomass on PVC coverslips was determined by adsorption of crystal violet. Crystal violet was then solubilized and $A_{600\ nm}$ measured. Crystal violet absorbance was normalized to culture density. Data are the mean of three independent experiments each of which contained three technical replicates (N = 3). Swim ring diameters were measure after single-colony inoculation into low density swim agar and incubation at room temperature. Data are the mean of nine independent experiments (N = 9). (B) The ability of plasmid-borne wild-type PdhS2 (p-*pdhS2*), the kinase-null allele (p-*pdhS2* (K^-P^+)), or the phosphatase-null allele (p-*pdhS2* (K^+P^-)) to complement the Δ*pdhS2* biofilm formation (black bars) and swimming motility (white bars) phenotypes was evaluated using P_{lac}-driven expression of each allele. Experiments were performed and data analyzed as described for (A) above. (C) The effect of plasmid-borne wild-type PdhS2 (p-*pdhS2*), the kinase-null allele (p-*pdhS2* (K^-P^+)), or the phosphatase-null allele (p-*pdhS2* (K^+P^-)) on biofilm formation (black bars) and swimming motility (white bars) when expressed from the P_{lac} promoter in the Δ*divK* mutant background was evaluated as in (A) and (B) above. For presentation all data are normalized to WT and expressed as %WT ± standard error of the mean (S.E.).

Figure 3. PdhS2 and DivJ are polarly localized in *A. tumefaciens*. Time-lapse microscopy of a C-terminal green fluorescent protein fusion to PdhS2 (A) and DivJ (B).

Phase and fluorescent images were acquired sequentially and overlaid. Time between panels is 40 minutes. To the right of each image is a cartoon interpretation of the image.

Figure 4. PdhS2 impacts CtrA abundance but not turnover kinetics. (A) Steady-state CtrA levels in indicated strains as determined via SDS-PAGE followed by immunoblotting with rabbit anti-$CtrA_{Cc}$ primary and IRDye 800CW-conjugated goat anti-rabbit secondary antibodies. (B) Proteolytic turnover of CtrA following translational arrest with chloramphenicol. Aliquots were removed at the indicated time points, lysed, and stored frozen at -20 ºC. CtrA levels were then determined via SDS-PAGE followed by immunoblotting, as described for (A) above. Blots were imaged using an LI-COR Odyssey Classic infrared imaging system and band intensities quantified with the Odyssey Classic software. Protein concentrations for each sample were normalized prior to electrophoresis.

Figure 5. PdhS2 activity intersects with the activity of multiple diguanylate cyclases. (A) Biofilm formation was quantified for the wild-type (WT) and indicated mutant strains as described in Figure 2. PleD, DgcA, DgcB have demonstrated diguanylate cyclase enzymatic activity. Thus far conditions under DgcC is active have yet to be identified. $P < 0.05$ compared to WT ([a]), D*pdhS2* ([b]), or corresponding diguanylate cyclase ([c]). (B) The effect on biofilm formation of plasmid-borne expression of wild-type *dgcB* (p-*dgcB*) or a catalytic mutant allele of *dgcB* (p-*dgcB**) was evaluated. Expression of each *dgcB* allele was driven by the P_{lac} promoter. Biofilm formation was evaluated as described in Figure 2. (*) = $P < 0.05$ compared to vector alone.

Figure S1. A combined kinase- and phosphatase-null PdhS2 mutant allele has little effect on biofilm formation or swimming motility. The ability of plasmid-borne expression of a kinase- and phosphatase- null allele of *pdhS2* (p-*pdhS2* (K^-P^-)) to complement the Δ*pdhS2* phenotypes was compared against the wild-type *pdhS2* allele (p-*pdhS2*). Biofilm formation (black bars) and swimming motility (white bars) were evaluated as in Figure 2.

Figure S2. The PdhS kinases are not entirely redundant in regulating biofilm formation. Biofilm formation was evaluated in the wild-type (WT) and indicated mutant strains as described in Figure 2.

Figure S3. PdhS2 regulation of swimming motility is independent of diguanylate cyclase activity. (A) Swimming motility of the wild-type (WT) and indicated mutant strains was evaluated as described in Figure 2. $P < 0.05$ compared to WT ([a]), D*pdhS2* ([b]), or corresponding diguanylate cyclase ([c]). (B) The effect on swimming motility of plasmid-borne expression of wild-type *dgcB* (p-*dgcB*) or a catalytic mutant allele of *dgcB* (p-*dgcB**) was evaluated. Expression of each *dgcB* allele was driven by the P_{lac} promoter. Biofilm formation was evaluated as described in Figure 2. (*) = $P < 0.05$ compared to vector alone.

Figure S4. The unipolar polysaccharide is required for PdhS2-dependent biofilm formation. (A) Biofilm formation was evaluated in the presence (+) or absence (-) of

pdhS2 in combination with the indicated polysaccharides. WT = wild-type, Cel^- = cellulose mutant, $ChvAB^-$ = cyclic-β-glucan mutant, $CrdS^-$ = curdlan mutant, $ExoA^-$ = succinoglycan mutant, UPP^- = unipolar polysaccharide mutant, EPS^- = mutant lacking all of the above polysaccharides. (B) Swimming motility was evaluated in the same strains as in (A). (*) = $P < 0.05$ compared to background strain.

Figure S5. PdhS2 does not affect global levels of cyclic-di-GMP. Cyclic-di-GMP levels were measured in whole cell extracts from equivalent ODs of the indicated strains. Data are from three independent experiments (N = 3).

Figure 1A

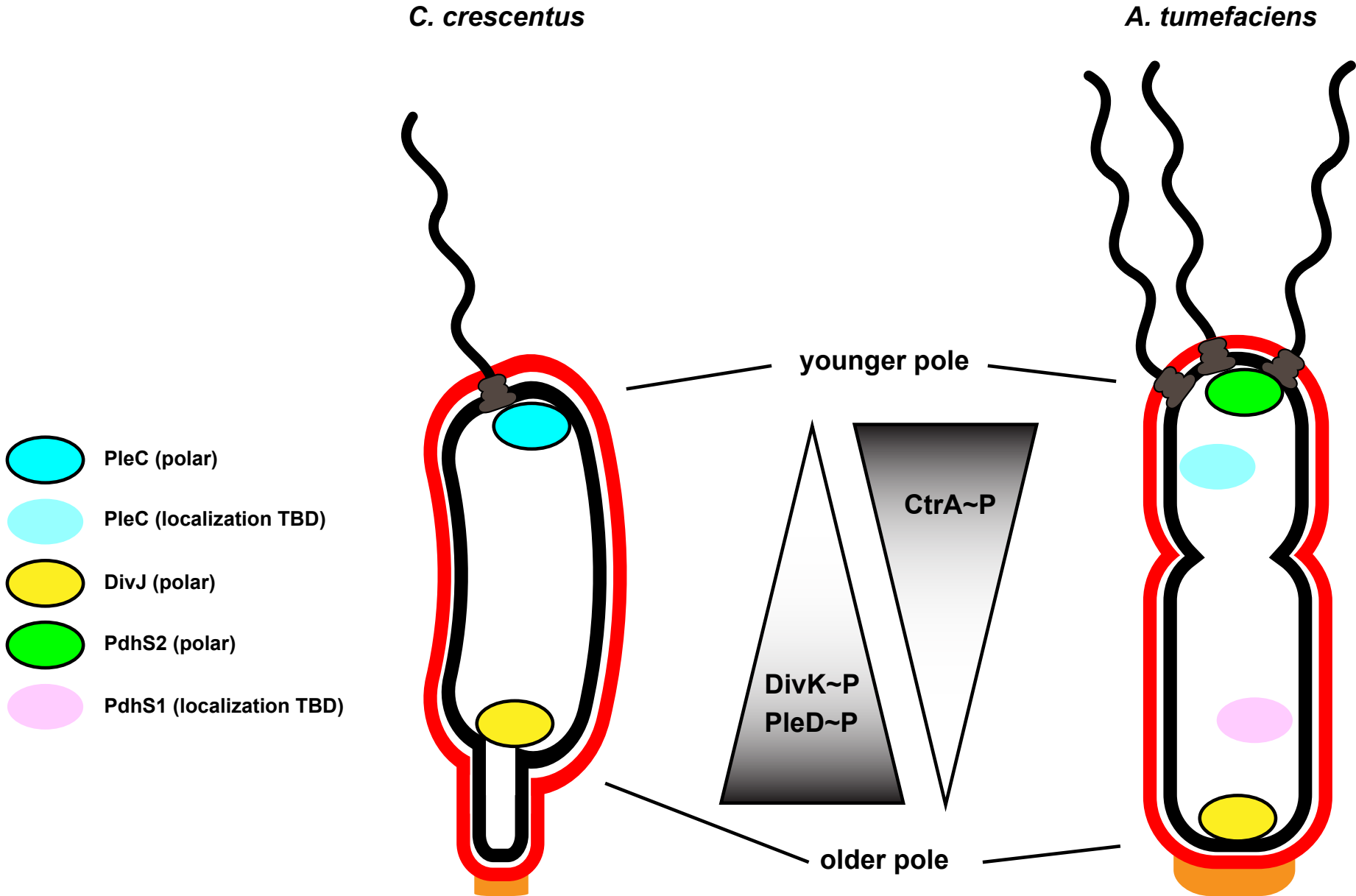
C. crescentus
A. tumefaciens
younger pole
older pole
CtrA~P
DivK~P
PleD~P
PleC (polar)
PleC (localization TBD)
DivJ (polar)
PdhS2 (polar)
PdhS1 (localization TBD)

Figure 1B

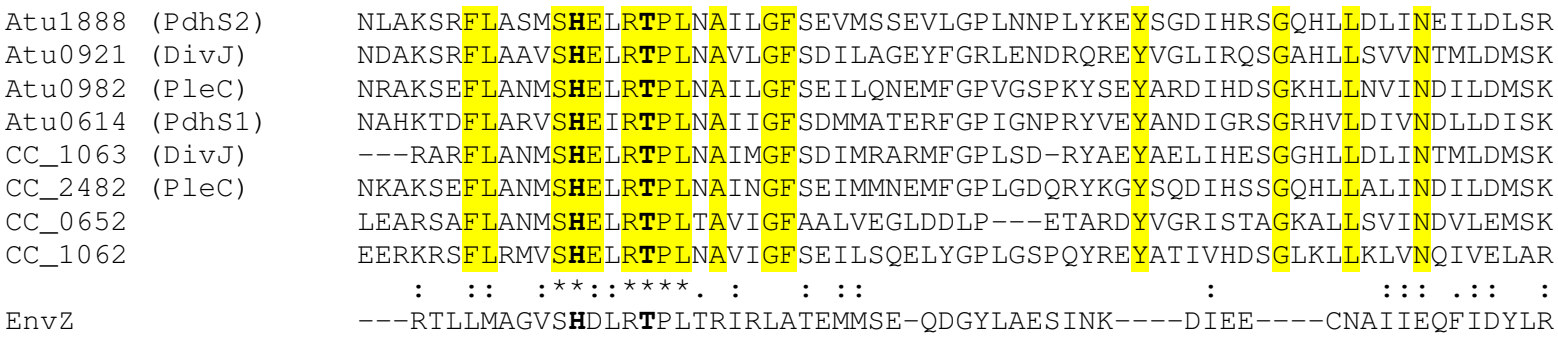
Atu1888 (PdhS2) NLAKSRFLASMSHELRTPLNAILGFSEVMSSEVLGPLNNPLYKEYSGDIHRSGQHLLDLINEILDLSR
Atu0921 (DivJ) NDAKSRFLAAVSHELRTPLNAVLGFSDILAGEYFGRLENDRQREYVGLIRQSGAHLLSVVNTMLDMSK
Atu0982 (PleC) NRAKSEFLANMSHELRTPLNAILGFSEILQNEMFGPVGSPKYSEYARDIHDSGKHLLNVINDILDMSK
Atu0614 (PdhS1) NAHKTDFLARVSHEIRTPLNAIIGFSDMMATERFGPIGNPRYVEYANDIGRSGRHVLDIVNDLLDISK
CC_1063 (DivJ) ---RARFLANMSHELRTPLNAIMGFSDIMRARMFGPLSD-RYAEYAELIHESGGHLLDLINTMLDMSK
CC_2482 (PleC) NKAKSEFLANMSHELRTPLNAINGFSEIMMNEMFGPLGDQRYKGYSQDIHSSGQHLLALINDILDMSK
CC_0652 LEARSAFLANMSHELRTPLTAVIGFAALVEGLDDLP---ETARDYVGRISTAGKALLSVINDVLEMSK
CC_1062 EERKRSFLRMVSHELRTPLNAVIGFSEILSQELYGPLGSPQYREYATIVHDSGLKLLKLVNQIVELAR
EnvZ ---RTLLMAGVSHDLRTPLTRIRLATEMMSE-QDGYLAESINK----DIEE----CNAIIEQFIDYLR

Figure 1C

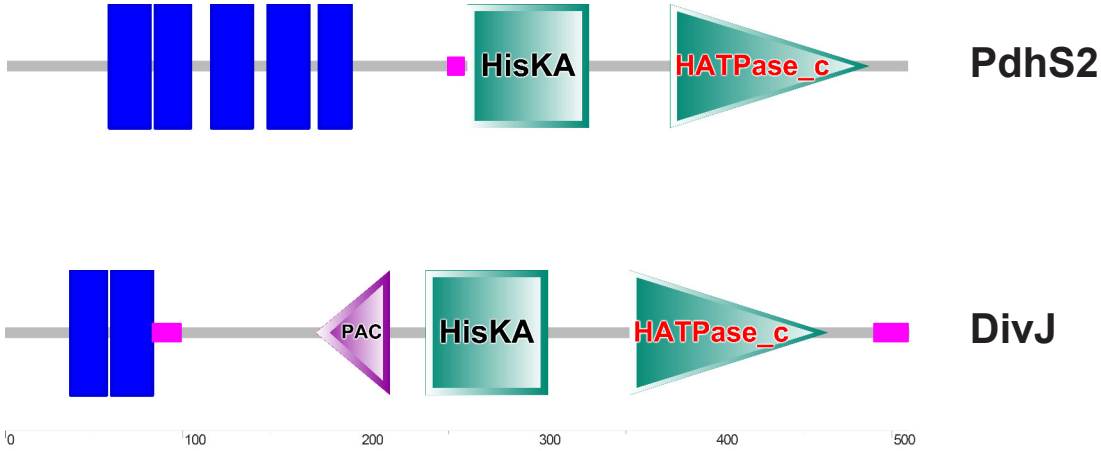
HisKA
HATPase_c
PdhS2
PAC
HisKA
HATPase_c
DivJ
0
100
200
300
400
500

Figure 2A

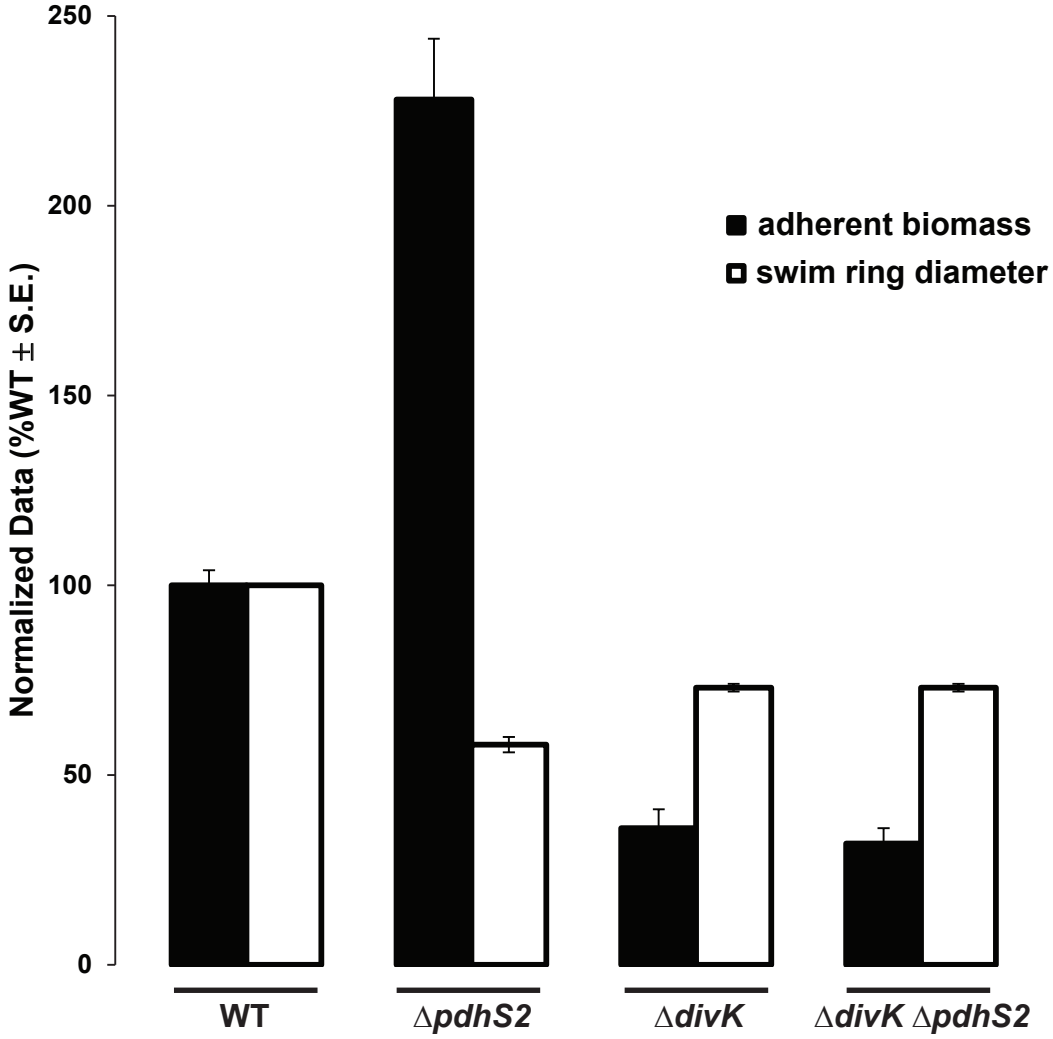
250
200
150
100
50
0
Normalized Data (%WT ± S.E.)
adherent biomass
swim ring diameter
WT
ΔpdhS2
ΔdivK
ΔdivK ΔpdhS2

Figure 2B

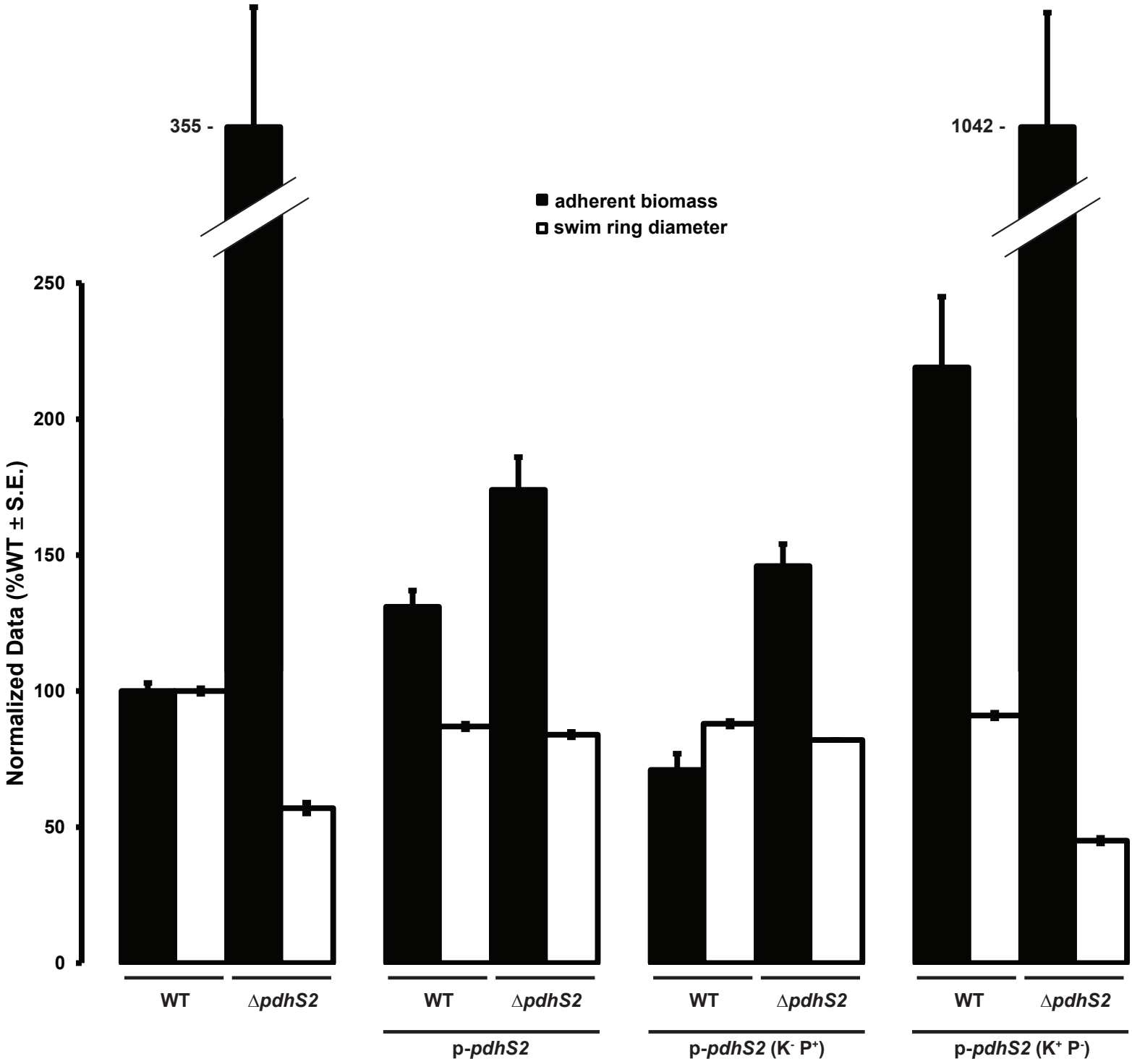
355 -
1042 -
adherent biomass
swim ring diameter
Normalized Data (%WT ± S.E.)
250
200
150
100
50
0
WT
ΔpdhS2
WT
ΔpdhS2
WT
ΔpdhS2
WT
ΔpdhS2
p-pdhS2
p-pdhS2 (K- P+)
p-pdhS2 (K+ P-)

Figure 2C

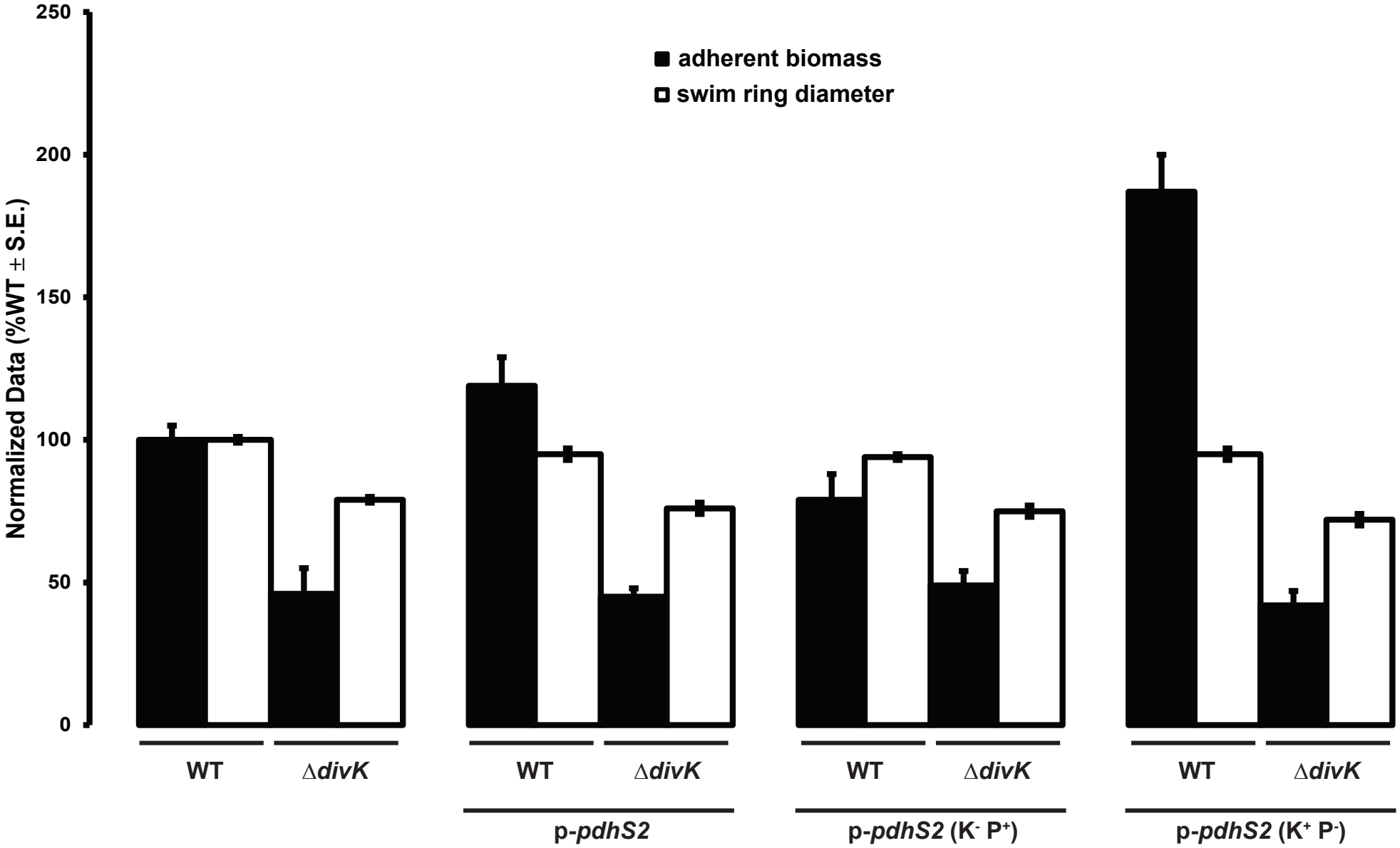
250
200
150
100
50
0
Normalized Data (%WT ± S.E.)
adherent biomass
swim ring diameter
WT
ΔdivK
WT
ΔdivK
WT
ΔdivK
WT
ΔdivK
p-pdhS2
p-pdhS2 (K- P+)
p-pdhS2 (K+ P-)

Figure 3

A

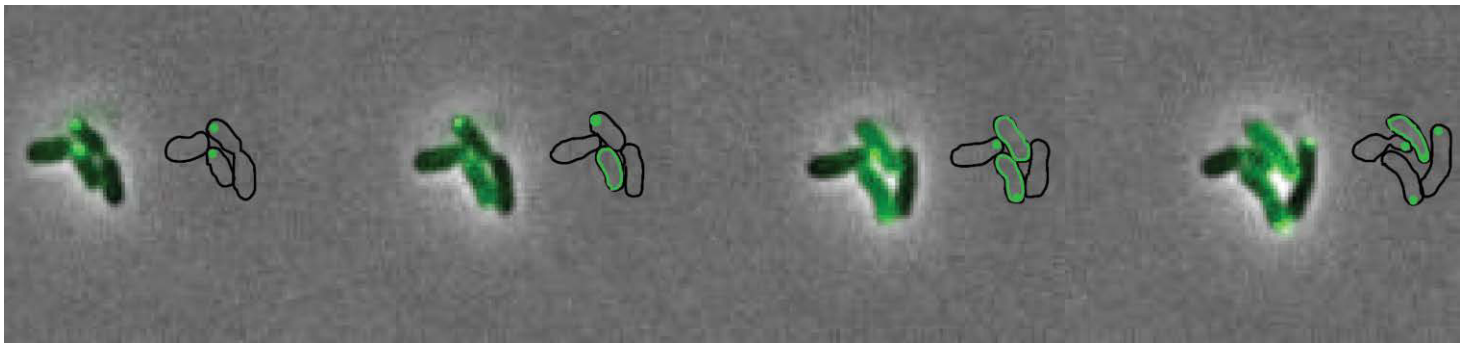

B

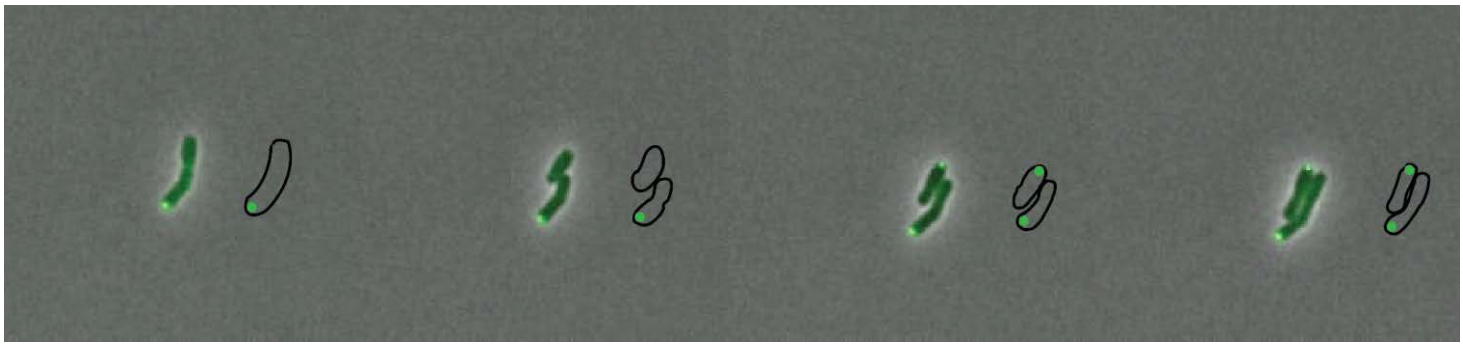

Figure 4A

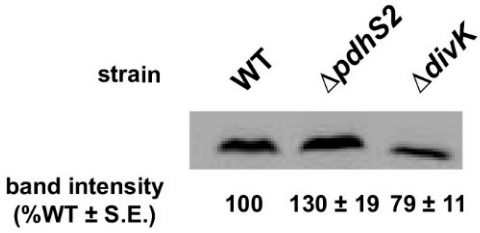

Figure 4B

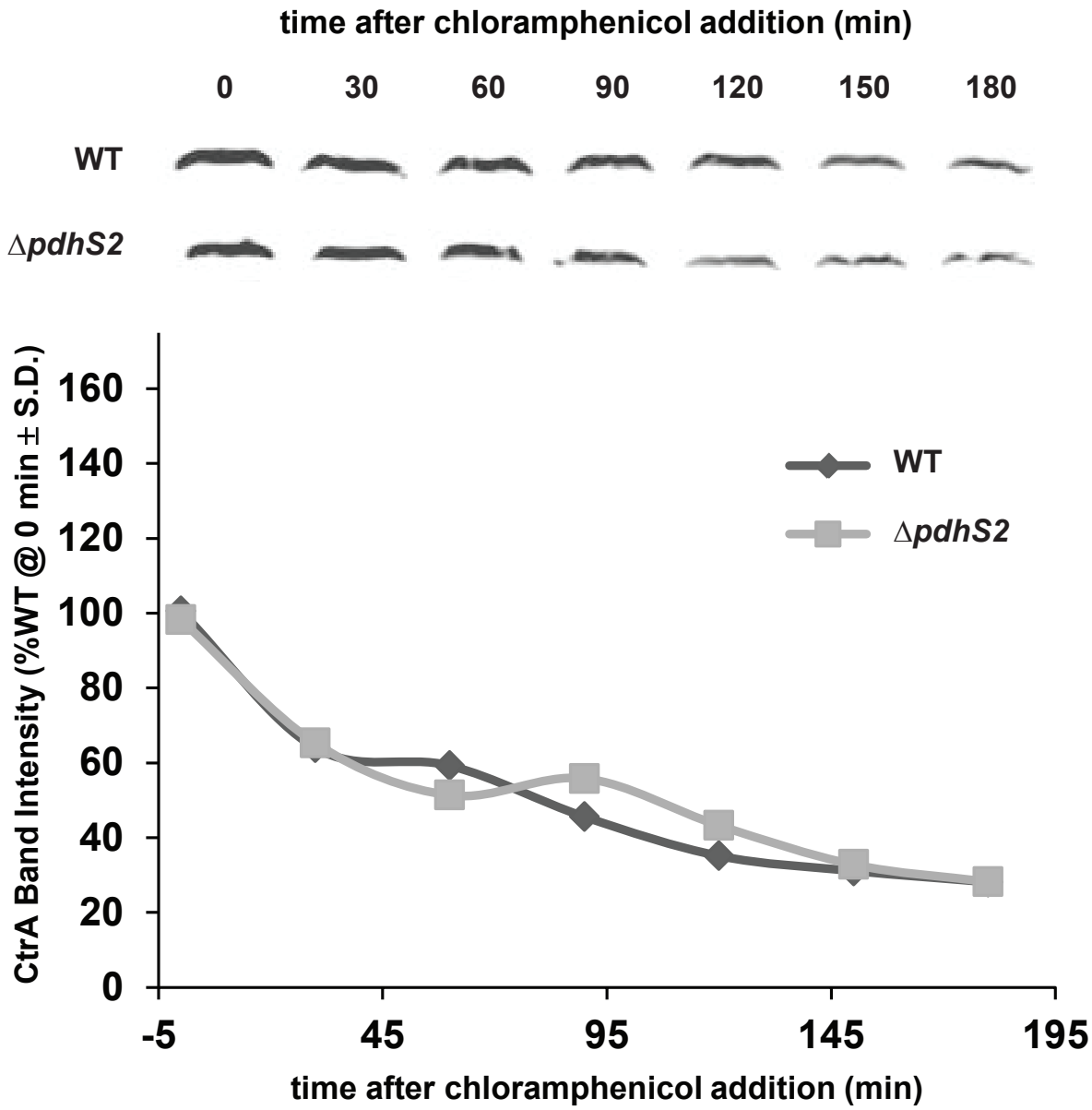
time after chloramphenicol addition (min)
0
30
60
90
120
150
180
WT
ΔpdhS2
CtrA Band Intensity (%WT @ 0 min ± S.D.)
160
140
120
100
80
60
40
20
0
WT
ΔpdhS2
-5
45
95
145
195
time after chloramphenicol addition (min)

Figure 5A

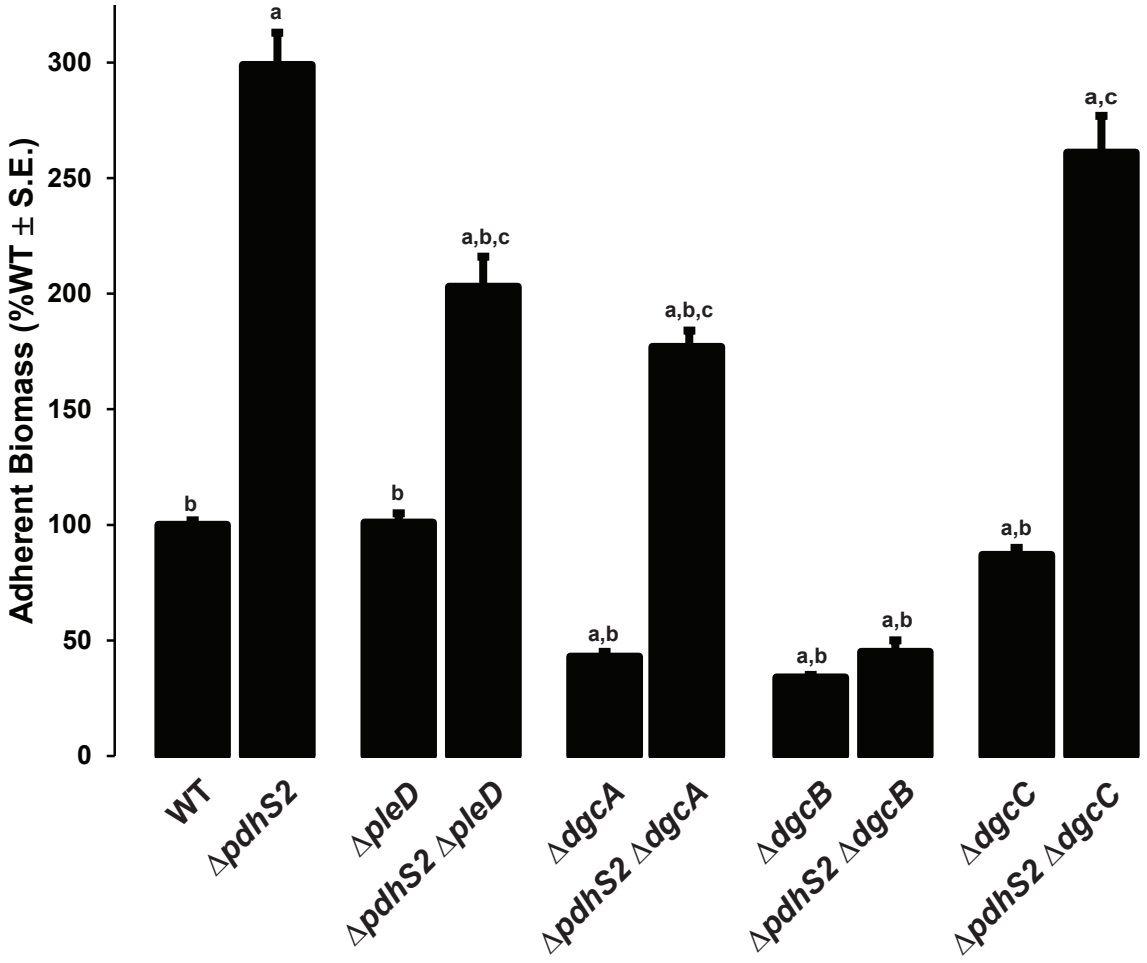
Adherent Biomass (%WT ± S.E.)
0
50
100
150
200
250
300
a
b
a,b,c
b
a,b,c
a,b
a,b
a,b
a,b
a,c
WT
ΔpdhS2
ΔpleD
ΔpdhS2 ΔpleD
ΔdgcA
ΔpdhS2 ΔdgcA
ΔdgcB
ΔpdhS2 ΔdgcB
ΔdgcC
ΔpdhS2 ΔdgcC

Figure 5B

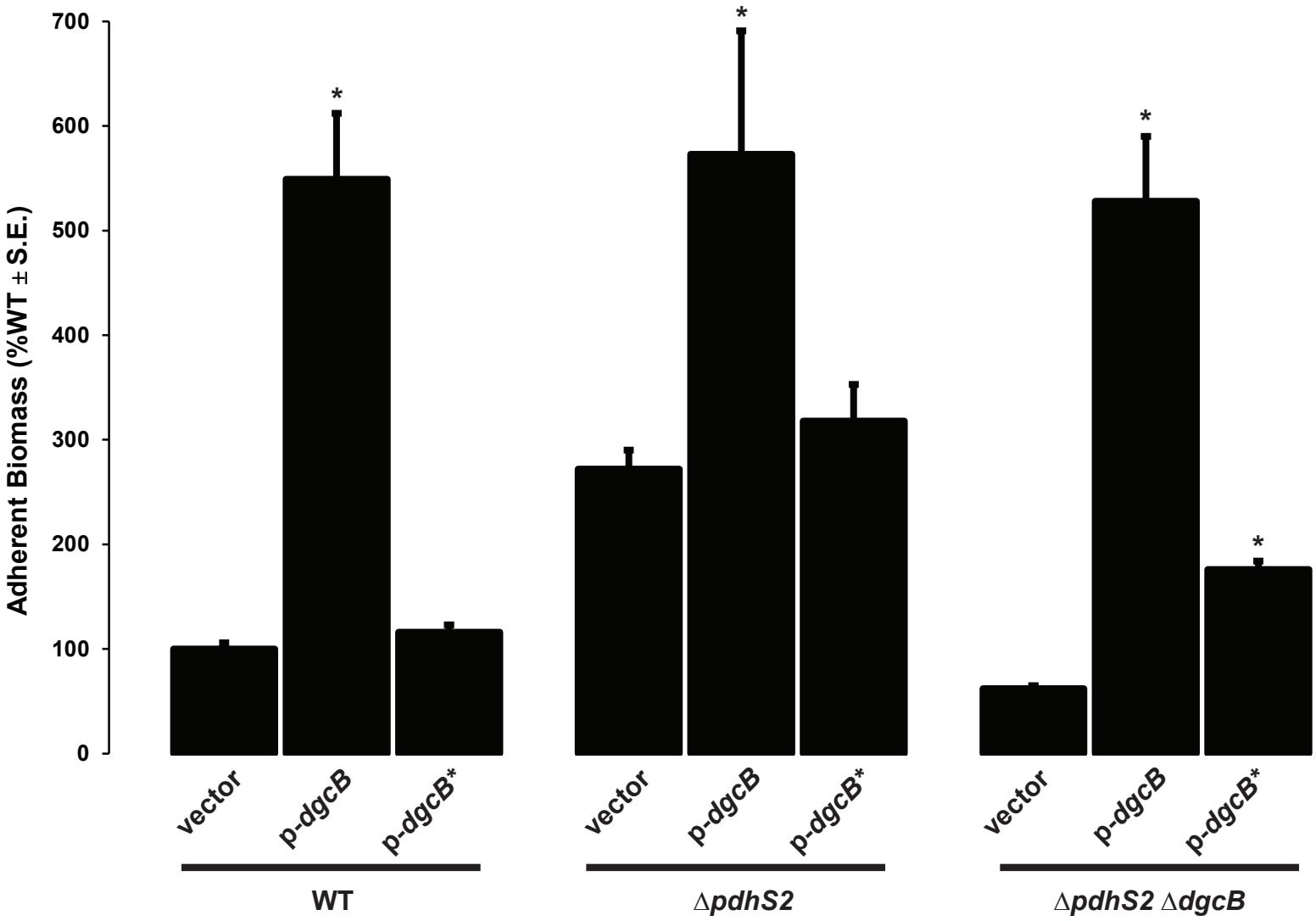
Adherent Biomass (%WT ± S.E.)
700
600
500
400
300
200
100
0
*
*
*
*
vector
p-dgcB
p-dgcB*
vector
p-dgcB
p-dgcB*
vector
p-dgcB
p-dgcB*
WT
ΔpdhS2
ΔpdhS2 ΔdgcB

SUPPLEMENTARY MATERIAL

Reciprocal control of motility and biofilm formation by the PdhS2 two-component sensor kinase of *Agrobacterium tumefaciens*

Jason E. Heindl, Daniel Crosby, Sukhdev Brar, Daniel Merenich, Aaron M. Buechlein, Eric L. Bruger, Christopher M. Waters and Clay Fuqua

Running title: *Agrobacterium PdhS2 regulates motility and biofilms*

1) Supplementary Figures – S1-S5

2) Supplementary Figure Legends

3) Supplementary Tables – S1-S3

4) Supplementary References

Figure S1

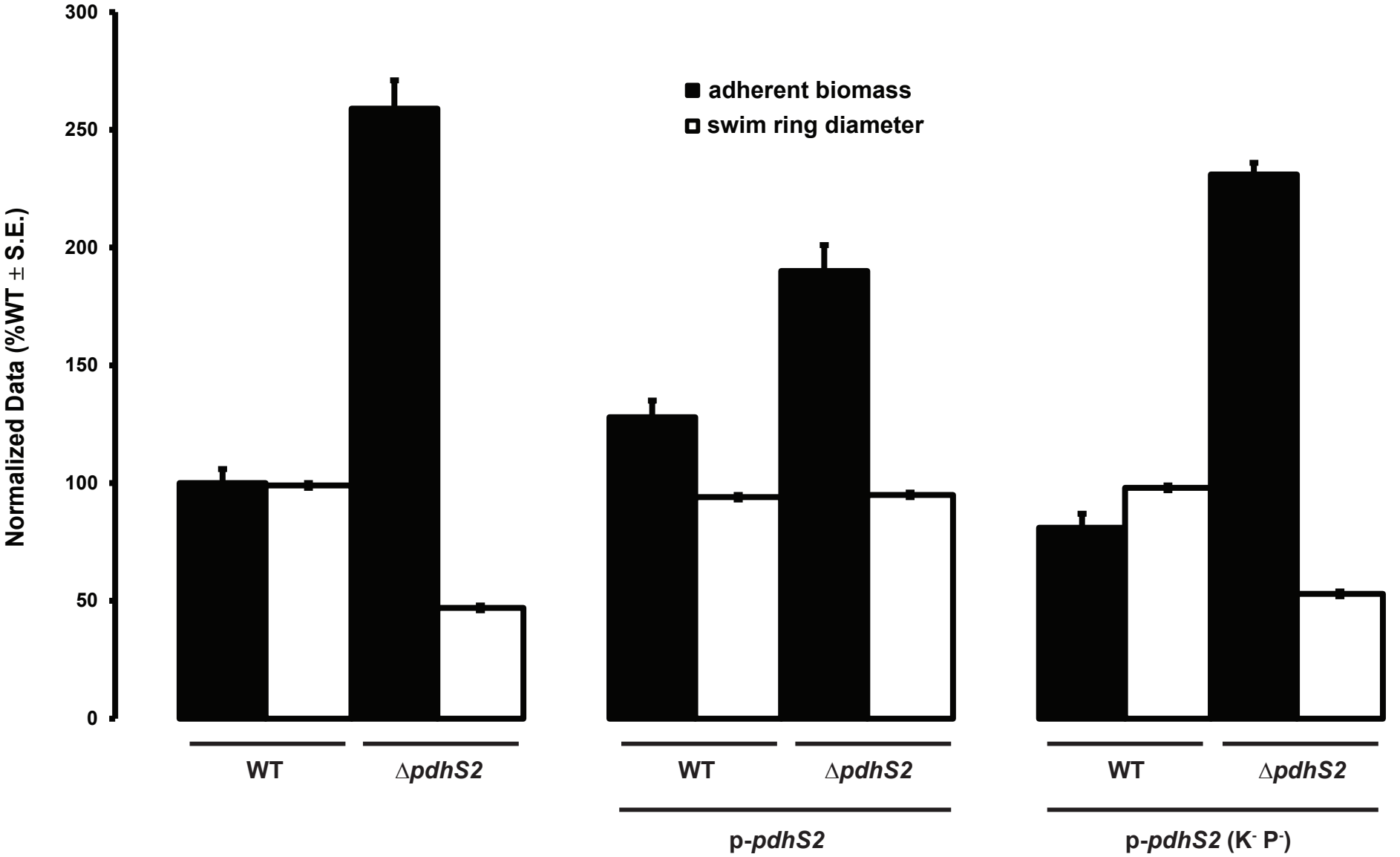
300
250
200
150
100
50
0
Normalized Data (%WT ± S.E.)
adherent biomass
swim ring diameter
WT
ΔpdhS2
WT
ΔpdhS2
p-pdhS2
WT
ΔpdhS2
p-pdhS2 (K- P-)

Figure S2

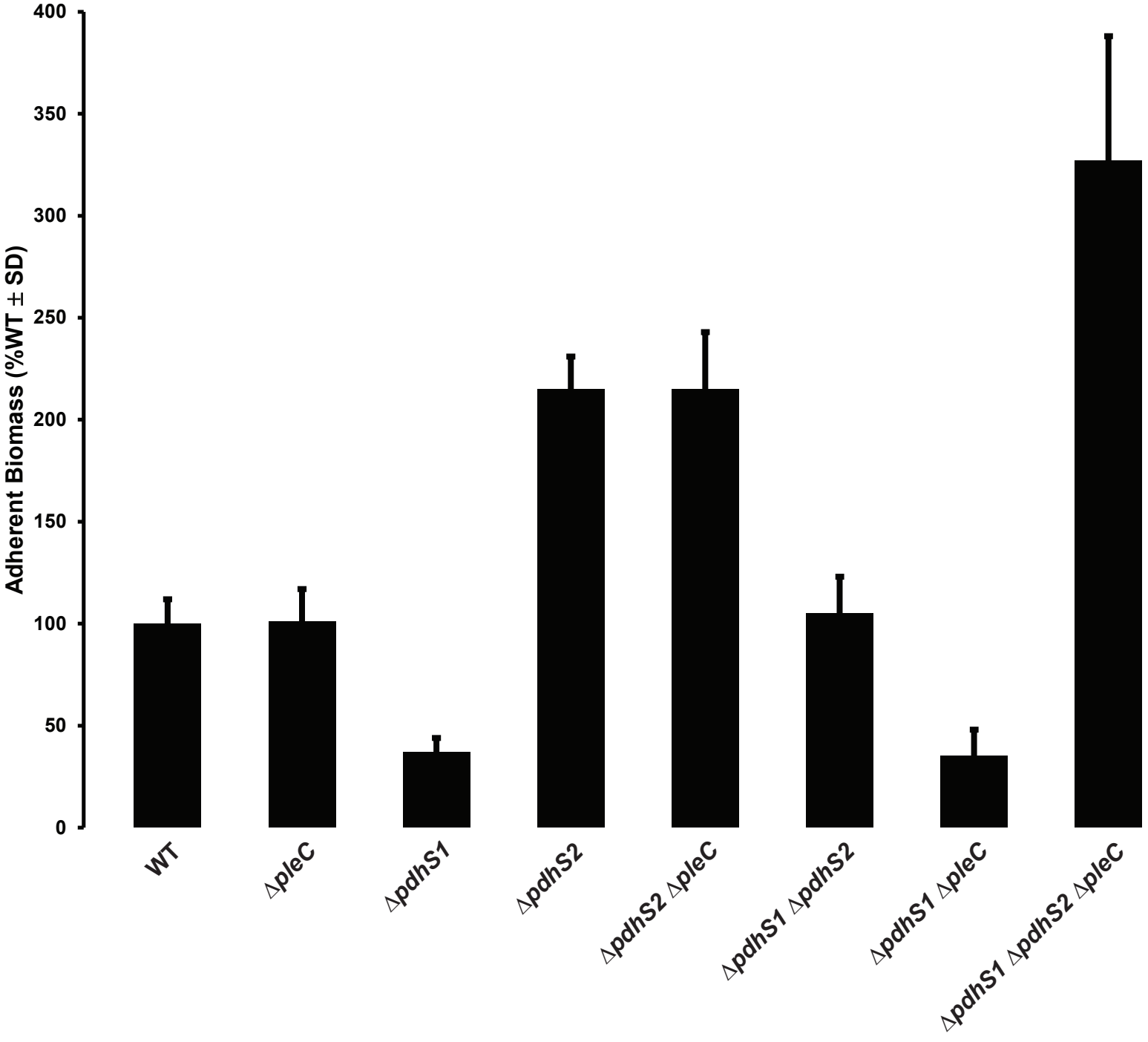
Adherent Biomass (%WT ± SD)
400
350
300
250
200
150
100
50
0
WT
ΔpleC
ΔpdhS1
ΔpdhS2
ΔpdhS2 ΔpleC
ΔpdhS1 ΔpdhS2
ΔpdhS1 ΔpleC
ΔpdhS1 ΔpdhS2 ΔpleC

Figure S3A

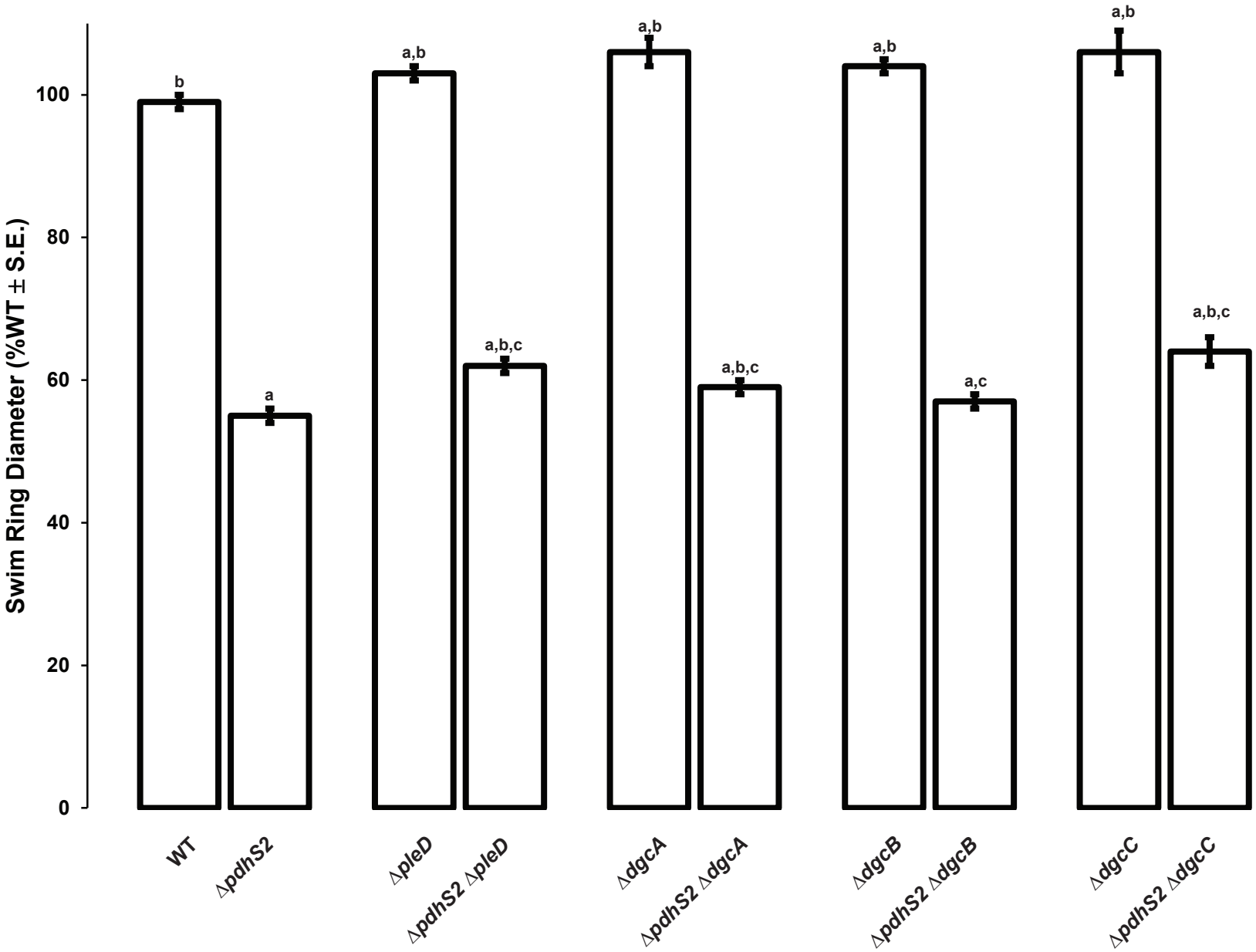
Swim Ring Diameter (%WT ± S.E.)
0
20
40
60
80
100
b
a
a,b
a,b,c
a,b
a,b,c
a,b
a,c
a,b
a,b,c
WT
ΔpdhS2
ΔpleD
ΔpdhS2 ΔpleD
ΔdgcA
ΔpdhS2 ΔdgcA
ΔdgcB
ΔpdhS2 ΔdgcB
ΔdgcC
ΔpdhS2 ΔdgcC

Figure S3B

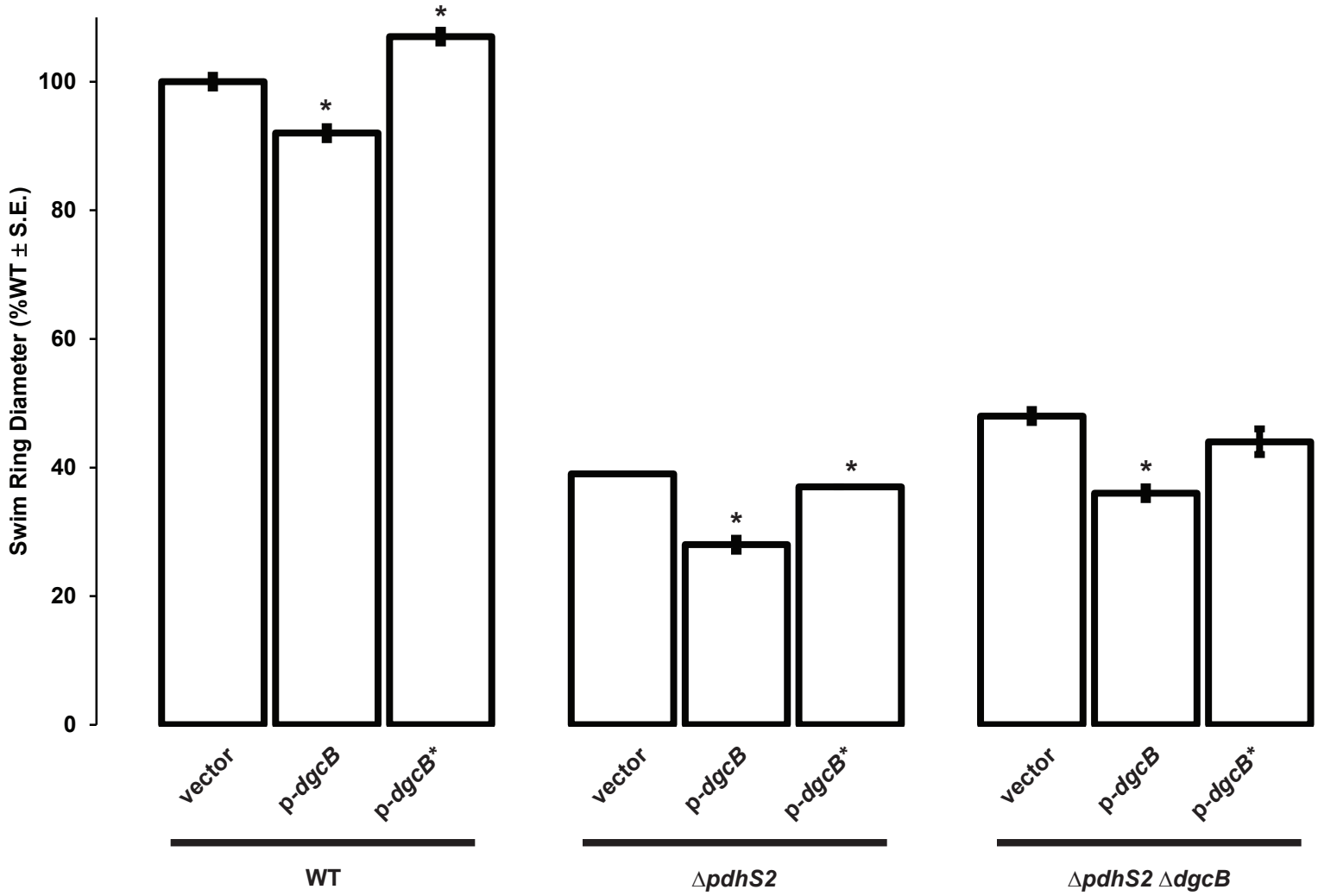
Swim Ring Diameter (%WT ± S.E.)
0
20
40
60
80
100
*
*
*
*
*
vector
p-dgcB
p-dgcB*
vector
p-dgcB
p-dgcB*
vector
p-dgcB
p-dgcB*
WT
ΔpdhS2
ΔpdhS2 ΔdgcB

Figure S4A

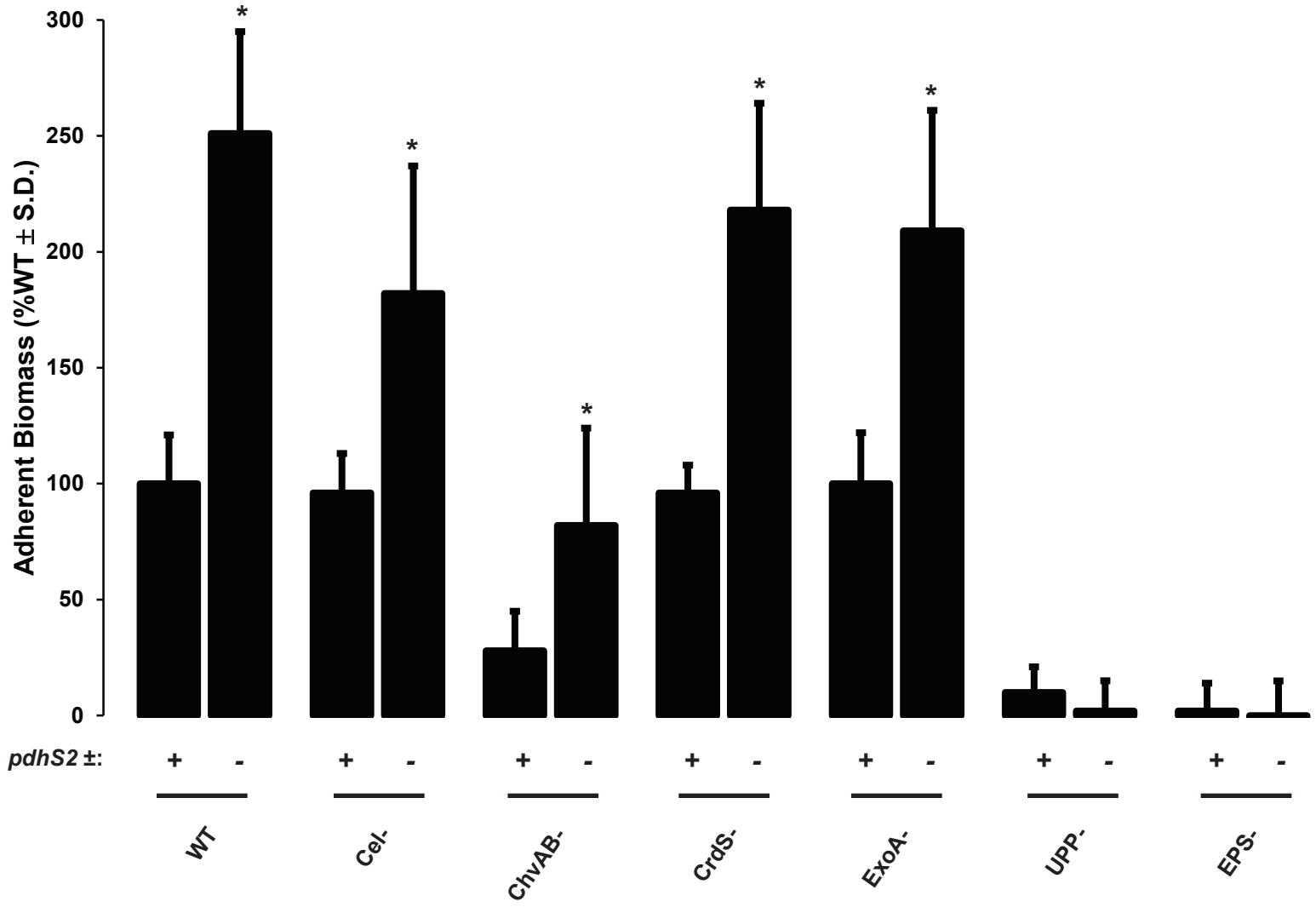
Adherent Biomass (%WT ± S.D.)
300
250
200
150
100
50
0
*
pdhS2 ±:
+
-
WT
Cel-
ChvAB-
CrdS-
ExoA-
UPP-
EPS-

Figure S4B

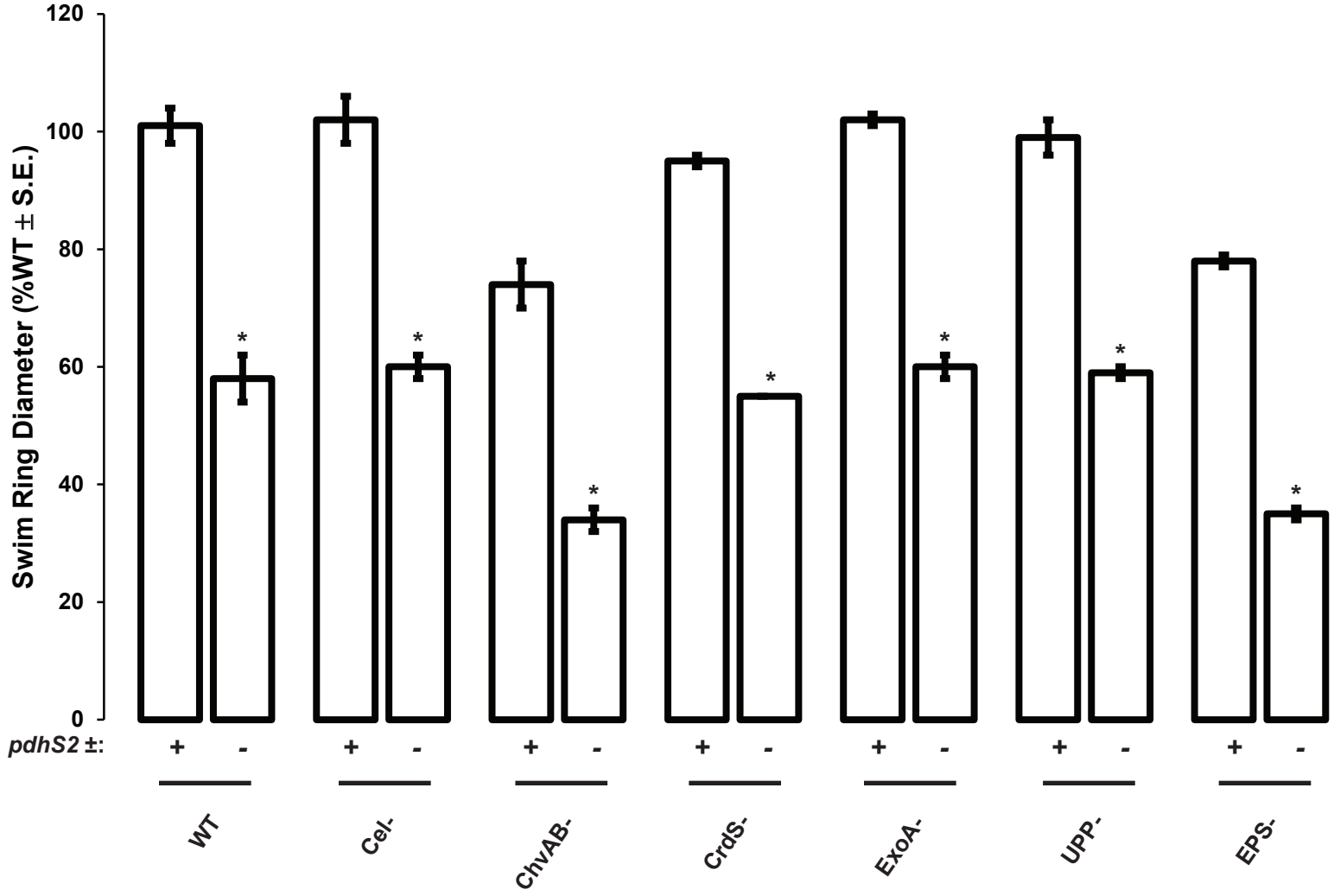
Swim Ring Diameter (%WT ± S.E.)
120
100
80
60
40
20
0
*
pdhS2 ±:
+
-
WT
Cel-
ChvAB-
CrdS-
ExoA-
UPP-
EPS-

Figure S5

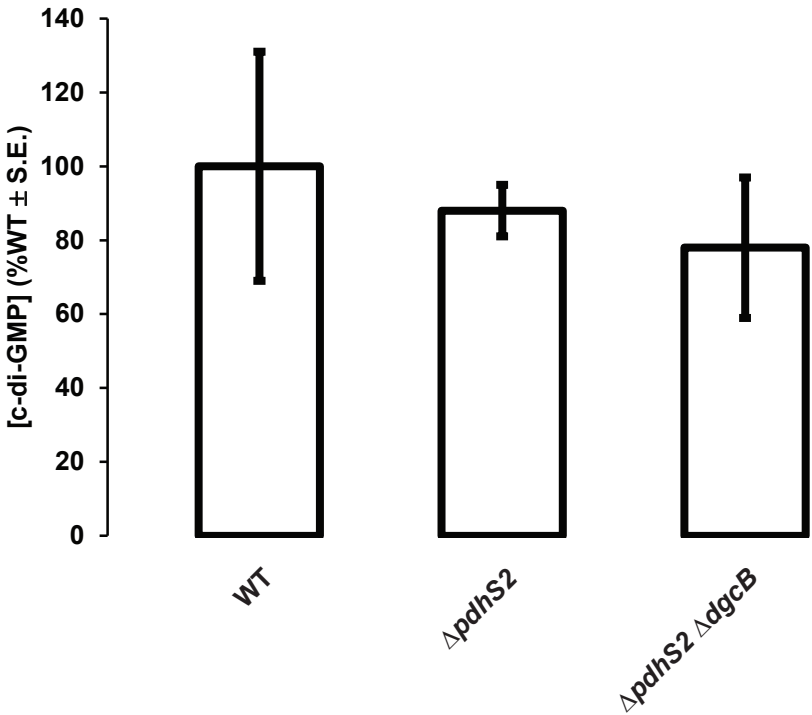

Figure S1. A combined kinase- and phosphatase-null PdhS2 mutant allele has little effect on biofilm formation or swimming motility. The ability of plasmid-borne expression of a kinase- and phosphatase- null allele of *pdhS2* (p-*pdhS2* (K^-P^-)) to complement the Δ*pdhS2* phenotypes was compared against the wild-type *pdhS2* allele (p-*pdhS2*). Biofilm formation (black bars) and swimming motility (white bars) were evaluated as in Figure 2.

Figure S2. The PdhS kinases are not entirely redundant in regulating biofilm formation. Biofilm formation was evaluated in the wild-type (WT) and indicated mutant strains as described in Figure 2.

Figure S3. PdhS2 regulation of swimming motility is independent of diguanylate cyclase activity. (A) Swimming motility of the wild-type (WT) and indicated mutant strains was evaluated as described in Figure 2. $P < 0.05$ compared to WT ([a]), D*pdhS2* ([b]), or corresponding diguanylate cyclase ([c]). (B) The effect on swimming motility of plasmid-borne expression of wild-type *dgcB* (p-*dgcB*) or a catalytic mutant allele of *dgcB* (p-*dgcB**) was evaluated. Expression of each *dgcB* allele was driven by the P_{lac} promoter. Biofilm formation was evaluated as described in Figure 2. (*) = $P < 0.05$ compared to vector alone.

Figure S4. The unipolar polysaccharide is required for PdhS2-dependent biofilm formation. (A) Biofilm formation was evaluated in the presence (+) or absence (-) of *pdhS2* in combination with the indicated polysaccharides. WT = wild-type, Cel^- =

cellulose mutant, ChvAB$^-$ = cyclic-β-glucan mutant, CrdS$^-$ = curdlan mutant, ExoA$^-$ = succinoglycan mutant, UPP$^-$ = unipolar polysaccharide mutant, EPS$^-$ = mutant lacking all of the above polysaccharides. (B) Swimming motility was evaluated in the same strains as in (A). (*) = $P < 0.05$ compared to background strain.

Figure S5. PdhS2 does not affect global levels of cyclic-di-GMP. Cyclic-di-GMP levels were measured in whole cell extracts from equivalent ODs of the indicated strains. Data are from three independent experiments (N = 3).

Table S1. Strains used in this study

Species	Strain	Relevant Characteristics	Source
A. tumefaciens	C58	Nopaline type strain, pAtC58, pTiC58	(1)
A. tumefaciens	C58-JEH076	Δ*pdhS2* (ΔAtu1888)	(2)
A. tumefaciens	C58-JEH128	Δ*pdhS2* Δ*pleD* (ΔAtu1888 ΔAtu1297)	This study
A. tumefaciens	C58-JEH130	Δ*pdhS2* Δ*dgcA* (ΔAtu1888 ΔAtu1257)	This study
A. tumefaciens	C58-JEH131	Δ*pdhS2* Δ*dgcB* (ΔAtu1888 ΔAtu1691)	This study
A. tumefaciens	C58-JEH132	Δ*pdhS2* Δ*dgcC* (ΔAtu1888 ΔAtu2179)	This study
A. tumefaciens	C58-JEH146	Δ*pdhS2* Δ*crdS* Δ*chvAB* Δ*cel* Δ*upp* Δ*exoA* (ΔAtu1888 ΔAtu3055-3057 ΔAtu2728-2730 ΔAtu3302-8187 ΔAtu1235-1240 ΔAtu4053)	This study
A. tumefaciens	C58-JEH147	Δ*pdhS2* Δ*upp* (ΔAtu1888 ΔAtu1235-1240)	This study
A. tumefaciens	C58-JEH148	Δ*pdhS2* Δ*cel* (ΔAtu1888 ΔAtu3302-8187)	This study

A. tumefaciens	C58-JEH149	Δ*pdhS2* Δ*crdS* (ΔAtu1888 ΔAtu3055-3057)	This study
A. tumefaciens	C58-JEH150	Δ*pdhS2* Δ*chvAB* (ΔAtu1888 ΔAtu2728-Atu2730)	This study
A. tumefaciens	C58-JEH151	Δ*pdhS2* Δ*exoA* (ΔAtu1888 ΔAtu4053)	This study
A. tumefaciens	C58-JEH153	Δ*divK* Δ*pdhS2* (ΔAtu1296 ΔAtu1888)	This study
A. tumefaciens	C58-JW7	Δ*divK* (ΔAtu1296)	(2)
A. tumefaciens	C58-JW8	Δ*pleD* (ΔAtu1297)	(2)
A. tumefaciens	C58-JX100	Δ*crdS* (ΔAtu3055-3057)	(3)
A. tumefaciens	C58-JX101	Δ*chvAB* (ΔAtu2728-2730)	(3)
A. tumefaciens	C58-JX102	Δ*cel* (ΔAtu3302-8187)	(3)
A. tumefaciens	C58-JX111	Δ*crdS* Δ*chvAB* Δ*cel* Δ*upp* Δ*exoA* (ΔAtu3055-3057 ΔAtu2728-2730 ΔAtu3302-8187 ΔAtu1235-1240 ΔAtu4053; “EPS$^-$”)	(3)
A. tumefaciens	C58-JX125	Δ*dgcA* (ΔAtu1257)	(4)
A. tumefaciens	C58-JX187	Δ*dgcB* (ΔAtu1691)	(4)
A. tumefaciens	C58-MLL2 A	Δ*exoA* (ΔAtu4053)	(5)
A. tumefaciens	C58-PMM26	Δ*upp* (ΔAtu1235-1240)	(3)

A. tumefaciens	C58-YW010	Δ*dgcC* (ΔAtu2179)	(4)
E. coli	S17-1 λ*pir*	RK2 *tra* regulon, *pir*, host for *pir*-dependent plasmids	(6)
E. coli	TOP10 F'	F'{*lac*I^q Tn*10* (Tet^R)} *mcr*A Δ(*mrr-hsd*RMS-*mcr*BC) Φ80*lacZ*ΔM15 Δ*lac*X74 *rec*A1 *ara*D139 Δ(*ara-leu*)7697 *gal*U *rps*L *end*A1 *nup*G	Thermo Fisher Scientific

Table S2. Plasmids used in this study

Plasmid name	Relevant characteristics	Source
pGEM-T Easy	PCR cloning vector; Amp^R	Promega
p*lacZ*/290	Broad host range plasmid carrying promoterless *lacZ* for transcriptional fusions; Tet^R	(7)
pNPTS138	colE1 origin; *sacB*; Km^R	gift of M. Alley
pRA301	Broad host range plasmid carrying promoterless *lacZ* for translational fusions; $Spec^R$	(8)
pSRKKm-tdTomato	pSRKKm vector with *tdTomato*	gift of P. Brown
pSRKGm	Broad host range vector containing P_{lac}; $lacI^q$; $lacZ\alpha^+$; Gm^R	(9)
p*ctrA*290	p*lacZ*/290 derivative with *C. crescentus ctrA* promoter	(10)
pDC001	pGEM-T Easy with full-length *pdhS2*$^{(CA811\text{-}812GC,}$	This study

	A823G) (PdhS2^{His271A,Thr275Ala} mutant)	
pDC002	pSRKGm with full-length *pdhS2*$^{(CA811-812GC, A823G)}$ (PdhS2^{His271A,Thr275Ala} mutant)	This study
pGZ22	p*lacZ*/290 derivative with *C. crescentus ccrM* promoter	(11)
pJEH026	pSRKGm with full-length *pdhS2*	(2)
pJEH021	pGEM-T Easy with full-length *pdhS2*	(2)
pJEH040	pNPTS138 derivative with *pdhS2* SOE deletion fragment	(2)
pJEH052	pGEM-T Easy with *pdhS2* lacking a stop codon	This study
pJEH053	pGEM-T Easy with *gfpmut3*	This study
pJEH054	pGEM-T Easy with *divJ* lacking a stop codon	This study

pJEH060	pSRKGm with a *pdhS2*::*gfpmut3* translational fusion	This study
pJEH078	pSRKGm with a *divJ*::*gfpmut3* translational fusion	This study
pJEH091	pGEM-T Easy with full-length *pdhS2*$^{(CA811-812GC)}$ (PdhS2^{His271Ala} mutant)	This study
pJEH092	pSRKGm with full-length *pdhS2*$^{(CA811-812GC)}$ (PdhS2^{His271Ala} mutant)	This study
pJEH099	pGEM-T Easy with full-length *pdhS2*$^{(A823G)}$ (PdhS2^{Thr275Ala} mutant)	This study
pJEH102	pSRKGm with full-length *pdhS2*$^{(A823G)}$ (PdhS2^{Thr275Ala} mutant)	This study
pJEH113	pGEM-T Easy with *A. tumefaciens ccrM* promoter	This study
pJEH115	pGEM-T Easy with *A. tumefaciens ctrA* promoter	This study

pJEH119	pGEM-T Easy with *A. tumefaciens pdhS1* promoter	This study
pJEH121	pRA301 with *A. tumefaciens ccrM* promoter	This study
pJEH122	pRA301 with *A. tumefaciens ctrA* promoter	This study
pJEH124	pRA301 with *A. tumefaciens pdhS1* promoter	This study
pJEH125	pGEM-T Easy with *pdhS2*$^{(CA811-812GC)}$ for C-terminal fusions	This study
pJEH126	pGEM-T Easy with *pdhS2*$^{(A823G)}$ for C-terminal fusions	This study
pJEH127	pSRKKm with *pdhS2*$^{(CA811-812GC)}$::*tdTomato* translational fusion	This study
pJEH128	pSRKKm with *pdhS2*$^{(A823G)}$::*tdTomato* translational fusion	This study

pJS70	p*lacZ*/290 derivative with *C. crescentus pilA* promoter	(12)
pJX158	pRA301 with *A. tumefaciens* Atu3318 promoter	(4)
pJX162	pRA301 with *A. tumefaciens dgcB* promoter	(4)
pJX520	pSRKGm with full-length *dgcB*	(4)
pJX521	pSRKGm with full-length *dgcB*$^{A767C, A770C}$ (DgcB$^{EE256-257AA}$ mutant)	(4)
pJZ383	pPZP201 derivative with P_{tac}::*gfpmut3*; Spec^{R}	(13)

Table S3. Primers used in this study

Primer	Sequence (5' – 3')	Use
JEH65	GAAGAACATATGAGTAAAAGCGTCAGCA	cloning *pdhS2* with NdeI site
JEH85	GATTTCGCGCGATCCCTTCGA	Internal primer for *pdhS2* locus
JEH87	GAGCAGATGCTGGCCGGA	Internal primer for *pdhS2* locus
JEH100	GCTCTGTTGAAGGCGGCCAA	External primer for *pdhS2* locus
JEH113	GCCGGTTTCATGCACACGCA	External primer for *pdhS2* locus
JEH146	GAAGAAGCTAGCGGCGAAAGACCGCCGG	cloning *pdhS2* w/o STOP and with NheI site
JEH147	GAAGAACATATGAGAGAAAAAGCGGTCGCA	cloning *divJ* with NdeI site
JEH148	GAAGAAGCTAGCGGCGATTTTCGCTTTCGCGG	cloning *divJ* w/o STOP and with NheI site
JEH149	GAAGAAGGTACCTTATTTGTATAGTTCATCCATGCCA	cloning *gfpmut3* with KpnI site
JEH150	GAAGAAGCTAGCATGAGTAAAGGAGAAGAACTT	cloning *gfpmut3* with NheI site
JEH245	CGTGCGCAGCTCGgcCGACATGGAAGCG	$pdhS2^{CA811-812GC}$ mutagenesis
JEH246	CGCTTCCATGTCGgcCGAGCTGCGCACG	$pdhS2^{CA811-812GC}$ mutagenesis
JEH261	CGCACGAGCTGCGCgCGCCGCTCAACGC	$pdhS2^{A823G}$ mutagenesis
JEH262	GCGTTGAGCGGCGcGCGCAGCTCGTGCG	$pdhS2^{A823G}$ mutagenesis
JEH272	GAGCTCGGGCGAAAGACCGCCG	reverse primer for cloning *pdhS2* w/o STOP and with SacI site
JEH282	GGTACCTGCCAGAATCGTTGCT	cloning *ccrM* promoter region, +222 bp to -9 bp from translational start, with KpnI site
JEH284	AAGCTTTGCTGCCATTGGTACT	cloning *ccrM* promoter region, +222 bp to -9 bp from translational start, with HindIII site
JEH285	GGTACCTTAACCTTTCGTTTACGGGCA	cloning *ctrA* promoter region, +328 bp to -9 bp from

		translational start, with KpnI site
JEH287	CTGCAGAACCCGCATAATTATCCCCTTT	cloning *ctrA* promoter region, +328 bp to -9 bp from translational start, with PstI site
JEH291	GGTACCATTTGCAAGTGCCTCTT	cloning *pdhS1* promoter region, +264 bp to -9 bp from translational start, with KpnI site
JEH293	AAGCTTGGCGGGCATGTCGAAA	cloning *pdhS1* promoter region, +264 bp to -9 bp from translational start, with HindIII site

REFERENCES

1. **Watson B, Currier TC, Gordon MP, Chilton MD, Nester EW**. 1975. Plasmid required for virulence of *Agrobacterium tumefaciens*. J. Bacteriol. **123**:255-264.
2. **Kim J, Heindl JE, Fuqua C**. 2013. Coordination of division and development influences complex multicellular behavior in Agrobacterium tumefaciens. PloS one **8**:e56682.
3. **Xu J, Kim J, Danhorn T, Merritt PM, Fuqua C**. 2012. Phosphorus limitation increases attachment in *Agrobacterium tumefaciens* and reveals a conditional functional redundancy in adhesin biosynthesis. Research in microbiology **163**:674-84.
4. **Xu J, Kim J, Koestler BJ, Choi JH, Waters CM, Fuqua C**. 2013. Genetic analysis of Agrobacterium tumefaciens unipolar polysaccharide production reveals complex integrated control of the motile-to-sessile switch. Molecular microbiology **89**:929-48.
5. **Tomlinson AD, Ramey-Hartung B, Day TW, Merritt PM, Fuqua C**. 2010. *Agrobacterium tumefaciens* ExoR represses succinoglycan biosynthesis and is required for biofilm formation and motility. Microbiology **156**:2670-81.
6. **Simon R, Priefer U, Puhler A**. 1983. A broad host range mobilization system for *in vivo* genetic engineering: transposon mutagenesis in gram negative bacteria. Bio/Technology (Nature Publishing Company) **Nov.**:784-791.
7. **Gober JW, Shapiro L**. 1992. A developmentally regulated *Caulobacter* flagellar promoter is activated by 3' enhancer and IHF binding elements. Mol Biol Cell **3**:913-26.
8. **Akakura R, Winans SC**. 2002. Constitutive mutations of the OccR regulatory protein affect DNA bending in response to metabolites released from plant tumors. J. Biol. Chem. **277**:5866-74.
9. **Khan SR, Gaines J, Roop RM, 2nd, Farrand SK**. 2008. Broad-host-range expression vectors with tightly regulated promoters and their use to examine the influence of TraR and TraM expression on Ti plasmid quorum sensing. Appl Environ Microbiol **74**:5053-62.
10. **Domian IJ, Reisenauer A, Shapiro L**. 1999. Feedback control of a master bacterial cell-cycle regulator. Proceedings of the National Academy of Sciences of the United States of America **96**:6648-53.
11. **Stephens CM, Zweiger G, Shapiro L**. 1995. Coordinate cell cycle control of a Caulobacter DNA methyltransferase and the flagellar genetic hierarchy. Journal of bacteriology **177**:1662-9.
12. **Skerker JM, Shapiro L**. 2000. Identification and cell cycle control of a novel pilus system in Caulobacter crescentus. The EMBO journal **19**:3223-34.
13. **Ramey BE, Matthysse AG, Fuqua C**. 2004. The FNR-type transcriptional regulator SinR controls maturation of *Agrobacterium tumefaciens* biofilms. Molecular microbiology **52**:1495-1511.